Universität Regensburg
Mathematik

Parametric approximation of Willmore flow and related geometric evolution equations

John W. Barrett, Harald Garcke and Robert Nürnberg

Preprint Nr. 22/2007

Parametric Approximation of Willmore Flow and Related Geometric Evolution Equations

John W. Barrett[†] Harald Garcke[‡] Robert Nürnberg[†]

Abstract

We present various variational approximations of Willmore flow in $\mathbb{R}^d$, $d = 2, 3$. As well as the classic Willmore flow, we consider also variants that are (a) volume preserving and (b) volume and area preserving. The latter evolution law is the so-called Helfrich flow. In addition, we consider motion by Gauß curvature. The presented fully discrete schemes are easy to solve as they are linear at each time level, and they have good properties with respect to the distribution of mesh points. Finally, we present numerous numerical experiments, including simulations for energies appearing in the modelling of biological cell membranes.

Key words. Willmore flow, Helfrich flow, Gauß curvature, fourth order parabolic problem, parametric finite elements, tangential movement

AMS subject classifications. 65M60, 65M12, 35K55

1 Introduction

The aim of this paper is to numerically approximate solutions of geometric evolution equations for hypersurfaces, which involve terms that are nonlinear in the principal curvatures. Prominent examples will be the Willmore flow, the Gauß curvature flow and several generalizations of the Willmore flow, which appear in the modelling of biological cell membranes. In this paper Γ is assumed to be a closed orientable hypersurface in $\mathbb{R}^d$, and we will mostly restrict ourselves to the practical cases of $d = 2$ or 3. Choosing a continuous normal field $\vec{\nu}$, the second fundamental tensor for a sufficiently smooth hypersurface Γ is then given by $\nabla_s \vec{\nu}$, where ∇_s is the surface gradient. We recall that $-\nabla_s \vec{\nu}(\vec{z})$, for any $\vec{z} \in \Gamma$, is a symmetric linear map that has a zero eigenvalue with eigenvector $\vec{\nu}$, and the remaining $(d-1)$ eigenvalues, $\varkappa_1, \ldots, \varkappa_{d-1}$, are the principal curvatures of Γ at $\vec{z}$; see e.g. Deckelnick, Dziuk, and Elliott (2005, p. 152). Hence $-\nabla_s \vec{\nu}(\vec{z})$ induces a linear

[†]Department of Mathematics, Imperial College London, London SW7 2AZ, UK
[‡]NWF I – Mathematik, Universität Regensburg, 93040 Regensburg, Germany

map $\mathcal{S} : T_{\vec{z}}\Gamma \to T_{\vec{z}}\Gamma$ on the tangent space $T_{\vec{z}}\Gamma$ for any $\vec{z} \in \Gamma$. The map $-\mathcal{S}$ is called the Weingarten map or shape operator. The mean curvature $\varkappa$ and the Gauß curvature $\mathcal{K}$ can now be stated as

$$\varkappa = \operatorname{tr} \mathcal{S} \qquad \text{and} \qquad \mathcal{K} = \det(\mathcal{S}), \tag{1.1}$$

where we, as is common in the literature, call the sum of the principal curvatures the mean curvature. We also note that our sign convention is such that a sphere has negative mean curvature if $\vec{\nu}$ is the unit outer normal; and from now on and throughout this paper, we assume that $\vec{\nu}$ denotes the outer normal. We remark already here, that it will be crucial to find discrete approximations for $\varkappa$, $\mathcal{K}$ and $\nabla_s \vec{\nu}$. At present in the literature only a simple and reliable discretization method exists for the mean curvature. Dziuk (1991) used a weak formulation of the identity

$$\Delta_s \vec{x} = \vec{\varkappa} \equiv \varkappa \vec{\nu} \tag{1.2}$$

in order to design a finite element method based on continuous piecewise linear elements, which was capable of approximating the mean curvature $\varkappa$ in a simple way. Here the operator $\Delta_s := \nabla_s \,.\, \nabla_s$ is the Laplace-Beltrami operator, $\vec{x}$ is a parametrisation of Γ and $\vec{\varkappa}$ is the so-called mean curvature vector. Dziuk (1991) used this approach to approximate solutions of the mean curvature flow

$$\mathcal{V} = \varkappa,$$

where we now assume that Γ is time dependent and where $\mathcal{V} = \vec{x}_t \,.\, \vec{\nu}$ is the normal velocity of the surface $\Gamma(t)$. Numerical approximations of the mean curvature flow are by now well established, and we refer to Deckelnick, Dziuk, and Elliott (2005) for a recent review on existing numerical approaches.

Numerical approximations of geometric evolution equations which involve terms nonlinear in the principal curvatures are far less well developed. One example is the Gauß curvature flow

$$\mathcal{V} = -\mathcal{K}, \tag{1.3}$$

which was first introduced by Firey (1974) as a model for the wearing process undergone by a pebble on a beach. As the Gauß curvature is the product of the principal curvatures, it is highly nonlinear. It appears at present that no satisfactory numerical approximation of the Gauß curvature flow exists, at least in a finite element framework.

Another prominent example in which highly nonlinear terms appear is the Willmore flow. The Willmore flow is the L^2-gradient flow of the Willmore energy

$$E(\Gamma) := \tfrac{1}{2} \int_\Gamma \varkappa^2 \,\mathrm{d}s, \tag{1.4}$$

see e.g. Willmore (1993) and Dziuk, Kuwert, and Schätzle (2002) for details. Minimizers and stationary points of the Willmore energy in a given topological class are not well understood at present, see Willmore (1993) and Hsu, Kusner, and Sullivan (1992). Of course, one can use the Willmore flow to try to obtain energy minimizers of the energy

(1.4). The energy (1.4), and variants involving also the Gauß curvature, appear as a bending energy in plate theory; which was actually first introduced by Germain and Kirchhoff. More recently, such energies have also appeared in the modelling of fluid membranes and vesicles, see Helfrich (1973), Seifert (1997) and the references therein. In order to derive the L^2-gradient flow of (1.4), let us now compute the first variation of (1.4). Let $\bigcup_{t\in[0,T]} \Gamma(t) \times \{t\}$ be an evolving hypersurface, see e.g. Gurtin (1993), and Deckelnick, Dziuk, and Elliott (2005), and let f be a quantity defined on the evolving hypersurface, which we extend to an open neighbourhood of the evolving surface. Then the following transport theorem holds, see e.g. Garcke and Wieland (2006),

$$\frac{\mathrm{d}}{\mathrm{d}t} \int_{\Gamma(t)} f \,\mathrm{d}s = \int_{\Gamma(t)} (\partial_t^0 f - f \varkappa \mathcal{V}) \,\mathrm{d}s \,. \tag{1.5}$$

Here

$$\partial_t^0 f := \partial_t f + (\nabla f) \,.\, \mathcal{V} \vec{\nu}$$

is the normal time derivative, and it can be shown that $\partial_t^0 f$ does not depend on the extension of f from the hypersurface to the neighbourhood. Hence we obtain as the first variation of E

$$\frac{\mathrm{d}}{\mathrm{d}t} E(\Gamma(t)) = \frac{\mathrm{d}}{\mathrm{d}t} \left[\tfrac{1}{2} \int_{\Gamma(t)} \varkappa^2 \,\mathrm{d}s \right] = \int_{\Gamma(t)} (\varkappa \partial_t^0 \varkappa - \tfrac{1}{2} \varkappa^2 \varkappa \mathcal{V}) \,\mathrm{d}s \,. \tag{1.6}$$

We have also the identity, see e.g. Gurtin and Jabbour (2002, p. 192, (2.19)) or Willmore (1993), Ecker (2004),

$$\partial_t^0 \varkappa = \Delta_s \mathcal{V} + \mathcal{V} |\nabla_s \vec{\nu}|^2 \,, \tag{1.7}$$

where $|\underline{\underline{A}}|^2 = \mathrm{tr}\,(\underline{\underline{A}}^T \underline{\underline{A}})$ is the Frobenius norm for any $\underline{\underline{A}} \in \mathbb{R}^{d\times d}$. Hence, we can use (1.7) in (1.6) and obtain after integration by parts that the L^2-gradient flow of E is given by

$$\mathcal{V} = -\Delta_s \varkappa - \varkappa |\nabla_s \vec{\nu}|^2 + \tfrac{1}{2} \varkappa^3 \,. \tag{1.8}$$

Since

$$|\nabla_s \vec{\nu}|^2 = \sum_{i=1}^{d-1} \varkappa_i^2 \,, \tag{1.9}$$

we obtain in particular that $|\nabla_s \vec{\nu}|^2 = \varkappa^2$ if $d = 2$ and $|\nabla_s \vec{\nu}|^2 = \varkappa^2 - 2\,\mathcal{K}$ if $d = 3$.

For a closed curve Γ, i.e. $d = 2$, on noting (1.9), the flow (1.8) simplifies to

$$\mathcal{V} = -\Delta_s \varkappa - \tfrac{1}{2} \varkappa^3 \,. \tag{1.10}$$

We note that for $d = 2$ the energy (1.4) can be reduced by scaling, as e.g. an expanding circle continuously reduces the energy E.

Realistic models for biological cell membranes lead to energies more general than (1.4). Classical bending energies for $d = 3$ also involve a term proportional to $\int_\Gamma \mathcal{K} \,\mathrm{d}s$. As long

as the topology is fixed, and as long as no boundary effects appear, this term can be discarded as

$$\int_\Gamma \mathcal{K}\,\mathrm{d}s = 4\,\pi\,(1-g) \tag{1.11}$$

is constant, where g is the genus of the surface.

In the original derivation of Helfrich (1973) a possible asymmetry in the membrane, originating e.g. from a different chemical environment, was taken into account. This led Helfrich to the energy

$$E(\Gamma) := \tfrac{1}{2}\int_\Gamma (\varkappa - \overline{\varkappa})^2\,\mathrm{d}s\,, \tag{1.12}$$

where $\overline{\varkappa} \in \mathbb{R}$ is the given so-called spontaneous curvature. Biological membranes consist of two layers of lipids. The number of lipid molecules is conserved and there are osmotic pressure effects, arising from the chemistry around the lipid. These both lead to constraints on the possible membrane configurations. Most models for bilayer membranes take *hard constraints on the total area and the enclosed volume* of the membrane into account. The fact that it is difficult to exchange molecules between the two layers imply that the total number of lipids in each layer is conserved and hence an area difference between the two layers will appear. The actual area difference can, to leading order, be described with the help of the total integrated mean curvature, see Seifert (1997). Now one can either incorporate this area difference by a hard constraint on the integrated mean curvature or one can penalize deviations from an optimal area difference. In the latter case, we obtain the energy

$$E(\Gamma) := \tfrac{1}{2}\int_\Gamma (\varkappa - \overline{\varkappa})^2\,\mathrm{d}s + \tfrac{\varrho}{2}\,(M - M_0)^2 \tag{1.13}$$

with $M := \int_\Gamma \varkappa\,\mathrm{d}s$ and given constants $\varrho > 0$, $M_0 \in \mathbb{R}$. For an evolving hypersurface we compute, using (1.5) and (1.7), that

$$\begin{aligned}\frac{\mathrm{d}}{\mathrm{d}t}\left[\tfrac{\varrho}{2}\,(M-M_0)^2\right] &= \varrho\,(M-M_0)\,\frac{\mathrm{d}}{\mathrm{d}t}\int_{\Gamma(t)} \varkappa\,\mathrm{d}s = \varrho\,(M-M_0)\int_{\Gamma(t)} (\partial_t^0\,\varkappa - \varkappa^2\,\mathcal{V})\,\mathrm{d}s\\ &= \varrho\,(M-M_0)\int_{\Gamma(t)} (|\nabla_s\,\vec{\nu}|^2 - \varkappa^2)\,\mathcal{V}\,\mathrm{d}s\,,\end{aligned}$$

where for $d = 3$ we have that $|\nabla_s\,\vec{\nu}|^2 - \varkappa^2 = -2\,\varkappa_1\,\varkappa_2 = -2\,\mathcal{K}$.

Now the gradient flow for (1.13), taking into account constraints for area and volume, is given by

$$\mathcal{V} = -\Delta_s\,\varkappa - (\varkappa - \overline{\varkappa})\,|\nabla_s\,\vec{\nu}|^2 + \tfrac{1}{2}\,(\varkappa-\overline{\varkappa})^2\,\varkappa - \varrho\,(M-M_0)\,(|\nabla_s\,\vec{\nu}|^2 - \varkappa^2) + \lambda\,\varkappa + \mu\,. \tag{1.14}$$

The equation (1.14) with $\mathcal{V} = 0$ characterizes stationary points of (1.13) taking volume and area constraints into account. The Lagrange multipliers, $\mu(t)$ and $\lambda(t)$, have to be chosen such that $\int_{\Gamma(t)} \mathcal{V}\,\mathrm{d}s = \int_{\Gamma(t)} \mathcal{V}\,\varkappa\,\mathrm{d}s = 0$, i.e. we obtain

$$\mu := \fint (\,(\varkappa - \overline{\varkappa})\,|\nabla_s\,\vec{\nu}|^2 + \varrho\,(M-M_0)\,(|\nabla_s\,\vec{\nu}|^2 - \varkappa^2) - \tfrac{1}{2}\,(\varkappa-\overline{\varkappa})^2\,\varkappa - \lambda\,\varkappa)\,,$$

where $⨍\eta := \frac{1}{|\Gamma(t)|}\int_{\Gamma(t)}\eta\,\mathrm{d}s$, and

$$\lambda := \frac{\int_{\Gamma(t)}\left[(I-⨍)\left((\varkappa-\overline{\varkappa})\,|\nabla_s\,\vec{\nu}|^2+\varrho\,(M-M_0)\,(|\nabla_s\,\vec{\nu}|^2-\varkappa^2)-\frac{1}{2}\,(\varkappa-\overline{\varkappa})^2\,\varkappa\right)\right]\varkappa\,\mathrm{d}s}{\int_{\Gamma(t)}|(I-⨍)\,\varkappa|^2\,\mathrm{d}s} - \frac{\int_{\Gamma(t)}|\nabla_s\,\varkappa|^2\,\mathrm{d}s}{\int_{\Gamma(t)}|(I-⨍)\,\varkappa|^2\,\mathrm{d}s}$$

if $\varkappa \not\equiv ⨍\varkappa$, and $\lambda = 0$ otherwise. In the case $\varrho = 0$, the evolution equation (1.14) reduces to the so-called Helfrich flow

$$\mathcal{V} = -\Delta_s\,\varkappa - (\varkappa-\overline{\varkappa})\,|\nabla_s\,\vec{\nu}|^2 + \tfrac{1}{2}\,(\varkappa-\overline{\varkappa})^2\,\varkappa + \lambda\,\varkappa + \mu, \tag{1.15}$$

i.e. the L^2-gradient flow of the energy (1.12) taking volume and area constraints into account. As mentioned above, in other models in the literature a hard constraint is also imposed on the area difference $M = \int_{\Gamma(t)}\varkappa\,\mathrm{d}s$, i.e. effectively ϱ is taken to be infinity, see Svetina and Zeks (1983). When $\overline{\varkappa} = 0$, this model is called *the bilayer-couple model* and its L^2-gradient flow is given as

$$\mathcal{V} = -\Delta_s\,\varkappa - \varkappa\,|\nabla_s\,\vec{\nu}|^2 + \tfrac{1}{2}\,\varkappa^3 + \gamma\,(|\nabla_s\,\vec{\nu}|^2-\varkappa^2) + \lambda\,\varkappa + \mu\,,$$

where μ, λ and γ are time dependent constants such that the volume, area and $M = \int_{\Gamma(t)}\varkappa\,\mathrm{d}s$ are conserved in time.

For theoretical results on the Willmore and Helfrich energies, and the corresponding flow problems, we refer to Willmore (1965), Pinkall and Sterling (1987), Di Carlo, Gurtin, and Podio-Guidugli (1992), Seifert (1997), Kuwert and Schätzle (2001), Gurtin and Jabbour (2002), Kuwert and Schätzle (2002), Bauer and Kuwert (2003), Kuwert and Schätzle (2004) and the references therein. Computational aspects of Willmore flow have been treated in Mayer and Simonett (2002), Rusu (2005), Clarenz, Diewald, Dziuk, Rumpf, and Rusu (2004), Deckelnick, Dziuk, and Elliott (2005), Deckelnick and Dziuk (2006) and the references therein.

Another flow, that we consider in this paper, is the generalized Gauß curvature flow, i.e.

$$\mathcal{V} = -\theta(\vec{\nu})\,\mathcal{K}^{\rho}\,. \tag{1.16}$$

Here $\theta : S^{d-1} \to \mathbb{R}$ is a mobility and $\rho \in \mathbb{R}$ is a given constant. The flow (1.16), for $\rho = 1$ and $\theta \equiv 1$ is the Gauß curvature flow (1.3). Moreover, the case $\theta(\vec{\nu}) \equiv c \in \mathbb{R}$ and $\rho = \frac{1}{d+1}$ plays an important role in differential geometry. Of course, for non integer values of ρ, the flow (1.16) is only well defined for surfaces without saddle points. We refer to Andrews (2000) and the references therein for more details, see also Tso (1985). Finally, the case $\theta(\vec{\nu}) = -1$ and $\rho = -1$ is also called the inverse Gauß curvature flow, see e.g. Schnürer (2006).

The only numerical work on the approximation of (1.16), that we are aware of, is Zhao and Xu (2006). In addition, in Ushijima and Yagisita (2005) the authors consider a suitable crystalline geometric flow for convex polyhedra in order to approximate (1.16).

The numerical approximations that we present here for Willmore flow, and these related flows, are extensions of our novel schemes for (nonlinear) mean curvature and surface diffusion flows of hypersurfaces, see Barrett, Garcke, and Nürnberg (2006); which, in comparison to other approaches, have good properties with respect to the distribution of mesh points. In this paper we extend on these ideas to allow for more control on the amount of tangential motion that is experienced by the discrete surfaces. As a result, the majority of the computations presented in this paper can be performed without a heuristical redistribution of mesh points. In order to compute solutions to the Willmore flow and the Gauß curvature flow, we had to come up with a new reliable discretization technique for the Weingarten map and the Gauß curvature in the context of piecewise linear continuous finite elements. Here it was crucial to introduce discrete vertex normals for polyhedral surfaces in order to compute the Weingarten map as its derivative. We refer to (2.3) and (2.7), below, for the details.

For later use we note that

$$\int_\Gamma \nabla_s \,.\, \vec{f}\,\mathrm{d}s = -\int_\Gamma \varkappa\,\vec{f}\,.\,\vec{\nu}\,\mathrm{d}s\,. \tag{1.17}$$

Here, and throughout, $\vec{f} = (f_1, \ldots, f_d)^T \in \mathbb{R}^d$ and $\nabla_s \vec{f} \in \mathbb{R}^{d\times d}$ with $(\nabla_s \vec{f})_{kl} = [\nabla_s f_k]_l$, $k, l = 1 \to d$; and $\nabla_s \,.\, \underline{\underline{A}} \in \mathbb{R}^d$ with $[\nabla_s \,.\, \underline{\underline{A}}]_l = \nabla_s \,.\, \vec{A}_l$, $l = 1 \to d$, for $\underline{\underline{A}}^T = [\vec{A}_1 \ldots \vec{A}_d] \in \mathbb{R}^{d\times d}$. We define also $\underline{\underline{A}} \,.\, \underline{\underline{B}} := \sum_{k,l=1}^d A_{kl}\, B_{kl}$ for $\underline{\underline{A}}, \underline{\underline{B}} \in \mathbb{R}^{d\times d}$.

On setting $\underline{\underline{w}} := \nabla_s \vec{\nu}$ we obtain from (1.17) with $\vec{f} = \underline{\underline{\varphi}}\,\vec{\nu}$, that

$$\int_\Gamma \underline{\underline{w}} \,.\, \underline{\underline{\varphi}}\,\mathrm{d}s = \int_\Gamma (\nabla_s \vec{\nu}) \,.\, \underline{\underline{\varphi}}\,\mathrm{d}s = -\int_\Gamma \vec{\nu} \,.\, (\nabla_s \,.\, \underline{\underline{\varphi}})\,\mathrm{d}s - \int_\Gamma (\varkappa\,\vec{\nu}) \,.\, (\underline{\underline{\varphi}}\,\vec{\nu})\,\mathrm{d}s\,; \tag{1.18}$$

so that, for example, Willmore flow in the presence of spontaneous curvature and no constraints can be written as

$$\mathcal{V} = -\Delta_s\,\varkappa - (\varkappa - \overline{\varkappa})\,|\underline{\underline{w}}|^2 + \tfrac{1}{2}\,(\varkappa - \overline{\varkappa})^2\,\varkappa, \qquad \varkappa\,\vec{\nu} = \Delta_s\,\vec{x}\,. \tag{1.19}$$

2 Finite element approximation

We introduce the following finite element approximation, that is based on the seminal paper by Dziuk (1991). Let $0 = t_0 < t_1 < \ldots < t_{M-1} < t_M = T$ be a partitioning of $[0, T]$ into possibly variable time steps $\tau_m := t_{m+1} - t_m$, $m = 0 \to M-1$. We set $\tau := \max_{m=0\to M-1} \tau_m$. Let Γ^m be a *polyhedral surface*, i.e. a union of non-degenerate triangles with no hanging vertices (see Deckelnick, Dziuk, and Elliott (2005, p. 164)), approximating the closed surface $\Gamma(t_m)$, $m = 0 \to M$. Following Dziuk (1991), we now parameterize the new closed surface Γ^{m+1} over Γ^m. Hence, given $\vec{X}^m$, a parameterization of Γ^m, we introduce the following finite element spaces. Let $\Gamma^m = \bigcup_{j=1}^J \overline{\sigma_j^m}$, where $\{\sigma_j^m\}_{j=1}^J$ is a family of mutually disjoint open triangles with vertices $\{\vec{q}_k^{\,m}\}_{k=1}^K$ and set

$h := \max_{j=1\to J} \operatorname{diam}(\sigma_j^m)$. Then for $m = 0 \to M-1$, let

$$\underline{V}(\Gamma^m) := \{\vec{\chi} \in C(\Gamma^m, \mathbb{R}^d) : \vec{\chi}|_{\sigma_j^m} \text{ is linear } \forall\ j = 1 \to J\} =: [V(\Gamma^m)]^d \subset H^1(\Gamma^m, \mathbb{R}^d),$$

where $V(\Gamma^m) \subset H^1(\Gamma^m, \mathbb{R})$ is the space of scalar continuous piecewise linear functions on Γ^m, with $\{\phi_k^m\}_{k=1}^K$ denoting the standard basis of $V(\Gamma^m)$. Similarly, we introduce the finite element space $\underline{\underline{V}}(\Gamma^m) \subset H^1(\Gamma^m, \mathbb{R}^{d\times d})$. Given a function $\eta^m \in V(\Gamma^m)$, we define $\pi^{m+1}\,\eta^m \in V(\Gamma^{m+1})$ by $(\pi^{m+1}\,\eta^m)(\vec{q}_k^{\,m+1}) := \eta^m(\vec{q}_k^{\,m})$ for $k = 1 \to K$, and similarly for the other finite element spaces. Throughout this paper, and where no confusion can arise, we will denote $\pi^{m+1}\,\eta^m$ also by η^m. An example is the slight abuse of notation $\vec{X}^m \in \underline{V}(\Gamma^{m+1})$, for the identity function $\vec{X}^m$ on Γ^m.

For scalar, vector and matrix functions $u, v \in L^2(\Gamma^m, \mathbb{R})$, $L^2(\Gamma^m, \mathbb{R}^d)$, $L^2(\Gamma^m, \mathbb{R}^{d\times d})$ we introduce the L^2 inner product $\langle\cdot,\cdot\rangle_m$ over the current polyhedral surface Γ^m, which is described by the vector function $\vec{X}^m$, as follows

$$\langle u, v\rangle_m := \int_{\Gamma^m} u\,.\,v \,\mathrm{d}s\,,$$

where $u\,.\,v$ denotes the usual inner product for vectors and matrices. In addition, if u, v are piecewise continuous, with possible jumps across the edges of $\{\sigma_j^m\}_{j=1}^J$, we introduce the mass lumped inner product $\langle\cdot,\cdot\rangle_m^h$ as

$$\langle u, v\rangle_m^h := \tfrac{1}{d}\sum_{j=1}^{J} |\sigma_j^m| \sum_{k=0}^{d-1} (u\,.\,v)((\vec{q}_{j_k}^{\,m})^-), \tag{2.1}$$

where $\{\vec{q}_{j_k}^{\,m}\}_{k=0}^{d-1}$ are the vertices of σ_j^m, and where we define $u((\vec{q}_{j_k}^{\,m})^-) := \lim_{\sigma_j^m \ni \vec{p} \to \vec{q}_{j_k}^{\,m}} u(\vec{p})$. Moreover $|\sigma_j^m|$ denotes the measure of σ_j^m. In addition, we introduce the outward unit normal $\vec{\nu}^m$ to Γ^m. Finally, we set $|\cdot|_{m(,h)}^2 := \langle\cdot,\cdot\rangle_m^{(h)}$.

We make the following very mild assumption.

($\mathcal{A}$) We assume for $m = 0 \to M$ that $|\sigma_j^m| > 0$ for all $j = 1 \to J$. For $k = 1 \to K$, let $\mathcal{T}_k^m := \{\sigma_j^m : \vec{q}_k^{\,m} \in \overline{\sigma_j^m}\}$ and set

$$\Lambda_k^m := \cup_{\sigma_j^m \in \mathcal{T}_k^m} \overline{\sigma_j^m} \qquad \text{and} \qquad \vec{\omega}_k^m := \frac{1}{|\Lambda_k^m|} \sum_{\sigma_j^m \in \mathcal{T}_k^m} |\sigma_j^m|\, \vec{\nu}_j^m\,. \tag{2.2}$$

Then we further assume that $\dim \operatorname{span}\{\vec{\omega}_k^m\}_{k=1}^K = d$, $m = 0 \to M-1$. In addition, we assume that $\vec{0} \notin \{\vec{\omega}_k^m\}_{k=1}^K$, $m = 1 \to M-1$.

For later purposes, we introduce discrete vertex normals on a given polyhedral surface Γ^m as follows. Let $\vec{\nu}^m \in \underline{V}(\Gamma^m)$ be such that

$$\vec{\nu}^m(\vec{q}_k^{\,m}) := \frac{\vec{\omega}_k^m}{|\vec{\omega}_k^m|}, \qquad k = 1 \to K\,, \tag{2.3}$$

which is well defined on noting assumption $(\mathcal{A})$.

Before we introduce our numerical approximations to the Willmore and related flows, we first mention a concept that will occur in all of them. Given $\vec{X}^m$, the identity function on Γ^m, we will seek the new position vector $\vec{X}^{m+1} \in \underline{V}(\Gamma^m)$ and the new mean curvature $\kappa^{m+1} \in V(\Gamma^m)$ such that they satisfy an approximation to an evolution equation and the following approximation of the identity (1.2):

$$\langle \kappa^{m+1}\, \vec{\nu}^m, \vec{\eta} \rangle_m^h + \langle \nabla_s\, \vec{X}^{m+1}, \nabla_s\, \vec{\eta} \rangle_m = 0 \qquad \forall\ \vec{\eta} \in \underline{V}(\Gamma^m)\,. \tag{2.4}$$

From now on, we will frequently refer to this fundamental "equation".

2.1 Willmore flow

The formulation (1.19), together with (1.18), leads to the following approximation of Willmore flow, in the presence of spontaneous curvature, for $d = 2$, 3. First, for $m \geq 0$, given $\{\vec{X}^m, \kappa^m\} \in \underline{V}(\Gamma^m) \times V(\Gamma^m)$, find $\underline{\underline{W}}^m \in \underline{\underline{V}}(\Gamma^m)$ such that

$$\langle \underline{\underline{W}}^m, \underline{\underline{\chi}} \rangle_m^h = -\langle \kappa^m\, \vec{\nu}^m, \underline{\underline{\chi}}\, \vec{\nu}^m \rangle_m^h - \langle \vec{\nu}^m, \nabla_s \cdot \underline{\underline{\chi}} \rangle_m \qquad \forall\ \underline{\underline{\chi}} \in \underline{\underline{V}}(\Gamma^m)\,, \tag{2.5}$$

where $\kappa^0 \in V(\Gamma^m)$ is suitably chosen; see Section 4. Then find $\{\vec{X}^{m+1}, \kappa^{m+1}\} \in \underline{V}(\Gamma^m) \times V(\Gamma^m)$ such that

$$\begin{aligned} \langle \frac{\vec{X}^{m+1} - \vec{X}^m}{\tau_m}, \chi\, \vec{\nu}^m \rangle_m^h - \langle \nabla_s\, \kappa^{m+1}, \nabla_s\, \chi \rangle_m - \tfrac{1}{2}\, \langle (\kappa^m - \overline{\varkappa})^2\, \kappa^{m+1}, \chi \rangle_m^h \\ = -\langle (\kappa^m - \overline{\varkappa})\, |\underline{\underline{W}}^m|^2, \chi \rangle_m^h \qquad \forall\ \chi \in V(\Gamma^m) \end{aligned} \tag{2.6}$$

and (2.4) hold. We note that for ease of notation, we will refer to the scheme (2.5), (2.6), (2.4) simply as scheme (2.5), (2.6), and similarly for all the remaining schemes in this paper. We note that the approximation (2.5) of the Weingarten map, $\underline{\underline{w}} = \nabla_s\, \vec{\nu}$, has also been considered in Heine (2007). In addition, we note that $\underline{\underline{W}}^m$ is not necessarily symmetric, whereas $\nabla_s\, \vec{\nu}$ is.

In view of (1.19), and on recalling (2.3), an alternative approximation is the following. Find $\{\vec{X}^{m+1}, \kappa^{m+1}\} \in \underline{V}(\Gamma^m) \times V(\Gamma^m)$ such that

$$\begin{aligned} \langle \frac{\vec{X}^{m+1} - \vec{X}^m}{\tau_m}, \chi\, \vec{\nu}^m \rangle_m^h - \langle \nabla_s\, \kappa^{m+1}, \nabla_s\, \chi \rangle_m - \tfrac{1}{2}\, \langle (\kappa^m - \overline{\varkappa})^2\, \kappa^{m+1}, \chi \rangle_m^h \\ = -\langle (\kappa^m - \overline{\varkappa})\, |\nabla_s\, \vec{v}^m|^2, \chi \rangle_m^h \quad \forall\ \chi \in V(\Gamma^m) \end{aligned} \tag{2.7}$$

and (2.4) hold. Again we note that $\nabla_s\, \vec{v}^m$ is not necessarily symmetric. However, in the following we require only approximations of $\mathrm{tr}\,(\nabla_s\, \vec{\nu})$ and $|\nabla_s\, \vec{\nu}|^2$.

2.2 Helfrich flow and other models

On recalling (1.15), it is straightforward to extend the approximations (2.5), (2.6) and (2.7) to suitable approximations for the Helfrich flow (1.15) and the more general flow (1.14). As will become clear later on, see Section 3, the former scheme is not very useful in practice. Hence here we only consider the extension of the scheme (2.7) to (1.14).

Find $\{\vec{X}^{m+1}, \kappa^{m+1}\} \in \underline{V}(\Gamma^m) \times V(\Gamma^m)$ such that

$$\begin{aligned}\langle \frac{\vec{X}^{m+1}-\vec{X}^m}{\tau_m}, \chi\,\vec{\nu}^m\rangle_m^h - \langle \nabla_s\,\kappa^{m+1}, \nabla_s\,\chi\rangle_m - \langle ([\lambda^m]_+ + \tfrac{1}{2}\,(\kappa^m-\overline{\varkappa})^2)\,\kappa^{m+1}, \chi\rangle_m^h = \\ - \langle (\kappa^m-\overline{\varkappa})\,|\nabla_s\,\vec{v}^m|^2, \chi\rangle_m^h - \varrho\,(\langle \kappa^m, 1\rangle_m - M_0)\,\langle |\nabla_s\,\vec{v}^m|^2 - (\kappa^m)^2, \chi\rangle_m^h \\ + [\lambda^m]_-\,\langle \kappa^m, \chi\rangle_m^h + \mu^m\,\langle 1, \chi\rangle_m \qquad \forall\ \chi \in V(\Gamma^m),\end{aligned} \tag{2.8}$$

and (2.4) hold, where

$$\mu^m := \tfrac{\langle (\kappa^m-\overline{\varkappa})\,|\nabla_s\,\vec{v}^m|^2 + \varrho\,(\langle \kappa^m,1\rangle_m - M_0)\,[|\nabla_s\,\vec{v}^m|^2 - (\kappa^m)^2] - \frac{1}{2}\,(\kappa^m-\overline{\varkappa})^2\,\kappa^m - \lambda^m\,\kappa^m, 1\rangle_m^h}{\langle 1,1\rangle_m}$$

and

$$\lambda^m := \tfrac{\langle (I-\mathit{f})\,((\kappa^m-\overline{\varkappa})\,|\nabla_s\,\vec{v}^m|^2 + \varrho\,(\langle \kappa^m,1\rangle_m - M_0)\,[|\nabla_s\,\vec{v}^m|^2 - (\kappa^m)^2] - \frac{1}{2}\,(\kappa^m-\overline{\varkappa})^2\,\kappa^m), \kappa^m\rangle_m^h - |\nabla_s\,\kappa^m|_m^2,}{|(I-\mathit{f})\,\kappa^m|_{m,h}^2}$$

if $|(I-\mathit{f})\,\kappa^m|_{m,h}^2 > 10^{-10}$ and $\lambda^m := 0$ otherwise, and where $[\lambda^m]_\pm := \pm\max\{\pm\lambda^m, 0\}$.

2.3 Gauß curvature flow

We propose the following scheme for the approximation of (1.16) for $d = 3$, on recalling from (1.9) that $\mathcal{K} = \frac{1}{2}\,(\varkappa^2 - |\nabla_s\,\vec{\nu}|^2)$. Find $\vec{X}^{m+1} \in \underline{V}(\Gamma^m)$ such that

$$\langle \frac{\vec{X}^{m+1}-\vec{X}^m}{\tau_m}, \chi\,\vec{\nu}^m\rangle_m^h = -\tfrac{1}{2^\rho}\,\langle \theta(\vec{\nu}^m)\,[\mathrm{tr}^2\,(\nabla_s\,\vec{v}^m) - |\nabla_s\,\vec{v}^m|^2]^\rho, \chi\rangle_m^h \qquad \forall\ \chi \in V(\Gamma^m) \tag{2.9}$$

and (2.4) hold. For later purposes, we define the employed approximation of Gauß curvature in (2.9) as $\mathcal{K}^m \in V(\Gamma^m)$ such that

$$\langle \mathcal{K}^m, \chi\,\vec{\nu}^m\rangle_m^h = \tfrac{1}{2}\,\langle \mathrm{tr}^2\,(\nabla_s\,\vec{v}^m) - |\nabla_s\,\vec{v}^m|^2, \chi\rangle_m^h \qquad \forall\ \chi \in V(\Gamma^m)\,. \tag{2.10}$$

Similarly, a scheme could be based on the following approximation of Gauß curvature, that employs (2.5) :

$$\langle \mathcal{K}^m, \chi\,\vec{\nu}^m\rangle_m^h = \tfrac{1}{2}\,\langle \mathrm{tr}^2\,(\underline{\underline{W}}^m) - |\underline{\underline{W}}^m|^2, \chi\rangle_m^h \qquad \forall\ \chi \in V(\Gamma^m)\,. \tag{2.11}$$

However, as the approximation $\underline{\underline{W}}^m$ from (2.5) in general is not close to the true Weingarten map $\underline{\underline{w}}(\cdot, t_m)$, see Section 4, this definition is not very practical for our purposes.

In Sullivan (2002), the following approximation for the Gauß curvature $\mathcal{K}^m \in V(\Gamma^m)$ of the polyhedral surface Γ^m is proposed:

$$\langle \mathcal{K}^m, \phi_k^m \rangle_m^h = 2\,\pi - \sum_{\sigma_j^m \in \mathcal{T}_k^m} \sphericalangle_k(\sigma_j^m)\,, \qquad k = 1 \to K\,, \tag{2.12}$$

where $\sphericalangle_k(\sigma_j^m)$ is the interior angle of the triangle σ_j^m at $\vec{q}_k^m$. The obvious adaption of the scheme (2.9) is then:

$$\langle \frac{\vec{X}^{m+1} - \vec{X}^m}{\tau_m}, \chi\,\vec{\nu}^m \rangle_m^h = -\langle \theta(\vec{\nu}^m)\,[\mathcal{K}^m]^\rho, \chi \rangle_m^h \qquad \forall\ \chi \in V(\Gamma^m)\,. \tag{2.13}$$

2.4 Reduced/Induced tangential motion

In this section we want to motivate an alternative to the equation (2.4), which will lead to some control on the amount of tangential movement for the discrete parameterizations. To this end, we recall the following schemes for the approximation of motion by surface diffusion, $\mathcal{V} = -\Delta_s\,\varkappa$, and mean curvature flow, $\mathcal{V} = \varkappa$, from Barrett, Garcke, and Nürnberg (2006). Find $\{\vec{X}^{m+1}, \kappa^{m+1}\} \in \underline{V}(\Gamma^m) \times V(\Gamma^m)$ such that

$$\langle \frac{\vec{X}^{m+1} - \vec{X}^m}{\tau_m}, \chi\,\vec{\nu}^m \rangle_m^h - \begin{cases} \langle \nabla_s\,\kappa^{m+1}, \nabla_s\,\chi \rangle_m^h \\ \langle \kappa^{m+1}, \chi \rangle_m^h \end{cases} = 0 \qquad \forall\ \chi \in W(\Gamma^m), \tag{2.14}$$

and (2.4) hold. We recall that (2.14) is unconditionally stable, i.e. it holds that

$$|\Gamma^{m+1}| + \tau_m \begin{cases} |\nabla_s\,\kappa^{m+1}|_m^2 \\ |\kappa^{m+1}|_{m,h}^2 \end{cases} \leq |\Gamma^m|\,, \tag{2.15}$$

which is a discrete analogue of

$$\frac{\mathrm{d}}{\mathrm{d}t}|\Gamma| \leq -\begin{cases} \int_\Gamma |\nabla_s\,\varkappa|^2\,\mathrm{ds} \\ \int_\Gamma \varkappa^2\,\mathrm{ds} \end{cases}. \tag{2.16}$$

For another unconditionally stable numerical approximation of the surface diffusion flow, we refer to Bänsch, Morin, and Nochetto (2005).

We define $\vec{\tau}_i^m := \sum_{k=1}^K \vec{\tau}_{i,k}^m\,\phi_k^m \in \underline{V}(\Gamma^m)$, where for each k $\{\vec{\nu}^m(\vec{q}_k^m), \vec{\tau}_{1,k}^m, \ldots, \vec{\tau}_{d-1,k}^m\}$ form an orthonormal basis of $\mathbb{R}^d$. We now introduce an alternative to (2.4), which allows us to either reduce the tangential motion in our schemes, or encourage tangential motion in selected directions. Let the coefficient vectors $0 \leq \alpha_i^m, \delta_i^m \in V(\Gamma^m)$, $i = 1 \to d-1$, and forcing terms $c_i^m \in V(\Gamma^m)$, $i = 1 \to d-1$, be given. Then, in addition to $\vec{X}^{m+1}$ and κ^{m+1}, find $\beta_i^{m+1} \in V(\Gamma^m)$, $i = 1 \to d-1$, such that for all $\chi \in V(\Gamma^m)$ and $\vec{\eta} \in \underline{V}(\Gamma^m)$

$$\langle \alpha_i^m\,\frac{\vec{X}^{m+1} - \vec{X}^m}{\tau_m}, \chi\,\vec{\tau}_i^m \rangle_m^h - \langle \alpha_i^m\,[\delta_i^m\,\beta_i^{m+1} + c_i^m], \chi \rangle_m^h = 0\ ,\ i = 1 \to d-1\,, \tag{2.17a}$$

$$\left\langle \kappa^{m+1}\,\vec{\omega}^m + \sum_{i=1}^{d-1} \alpha_i^m\,\beta_i^{m+1}\,\vec{\tau}_i^m, \vec{\eta} \right\rangle_m^h + \langle \nabla_s\,\vec{X}^{m+1}, \nabla_s\,\vec{\eta} \rangle_m = 0. \tag{2.17b}$$

Here we recall that $\langle \vec{\eta}, \chi\, \vec{\nu}^m \rangle_m^h = \langle \vec{\eta}, \chi\, \vec{\omega}^m \rangle_m^h$ for all $\vec{\eta} \in \underline{V}(\Gamma^m)$ and $\chi \in V(\Gamma^m)$.

Clearly, on replacing (2.4) in any of the schemes discussed in this paper with (2.17a,b) leads to a new family of schemes for the same evolution equations. E.g. (2.14), (2.17a,b) leads to a new scheme for surface diffusion. Note also that with the special choice $\alpha_i^m \equiv 0$, $i = 1 \to d-1$, this scheme collapses to the original scheme (2.14), (2.4), and similarly for the remaining approximations.

It is not difficult to show that the scheme (2.14), (2.17a,b) satisfies the following stability bound:

$$|\Gamma^{m+1}| + \tau_m \begin{cases} |\nabla_s\, \kappa^{m+1}|_m^2 \\ |\kappa^{m+1}|_{m,h}^2 \end{cases} + \tau_m \sum_{i=1}^{d-1} \langle \alpha_i^m\, [\delta_i^m\, \beta_i^{m+1} + c_i^m], \beta_i^{m+1} \rangle_m^h + \tfrac{1}{2}\, |\nabla_s\, (\vec{X}^{m+1} - \vec{X}^m)|_m^2 \leq |\Gamma^m|\,, \tag{2.18}$$

which means that the scheme is stable; in the sense that it satisfies a discrete analogue of (2.16), provided that

$$\sum_{i=1}^{d-1} \langle \alpha_i^m\, [\delta_i^m\, \beta_i^{m+1} + c_i^m]\, \beta_i^{m+1} \rangle_m^h + \tfrac{1}{2}\, |\nabla_s\, (\vec{X}^{m+1} - \vec{X}^m)|_m^2 \geq 0,$$

which is obviously guaranteed if $c_i^m \equiv 0$, $i = 1 \to d-1$. Then choosing $\delta_i^m \equiv 1$, $i = 1 \to d-1$, it follows intuitively from (2.18) that the tangential motion of $\vec{q}_k^m$ in the direction of $\vec{\tau}_{i,k}^m$ will be suppressed if $\alpha_i^m(\vec{q}_k^m)$ is large for any k. More generally, it is clear from (2.17a) that choosing $\delta_i^m \equiv 0$ and $\alpha_i^m > 0$ allows us to completely fix the tangential motion. However, stability then hinges on the sign of $c_i^m\, \beta_i^{m+1}$. These observations form the basis of our new ansatz to control tangential movement in the discrete evolution of geometric flows.

Altogether, we consider the following strategies in this paper.

$$\begin{aligned} &(i) \quad \alpha_i^m \equiv \alpha \in \mathbb{R}_{\geq 0},\ \delta_i^m \equiv 1,\ c_i^m \equiv 0; \\ &(ii) \quad \alpha_i^m \equiv \alpha \in \mathbb{R}_{>0},\ \delta_i^m \equiv \delta \in \mathbb{R}_{>0},\ c_i^m(\vec{q}_k^m) = \tfrac{1}{\tau_m}\, (\vec{z}_k^m - \vec{q}_k^m)\,.\, \vec{\tau}_{i,k}^m,\ k = 1 \to K; \\ &(iii) \quad \alpha_i^m \equiv 1,\ \delta_i^m \equiv 0,\ c_i^m(\vec{q}_k^m) = \tfrac{1}{\tau_m}\, (\vec{z}_k^m - \vec{q}_k^m)\,.\, \vec{\tau}_{i,k}^m, \quad k = 1 \to K; \end{aligned} \tag{2.19}$$

for $i = 1 \to d-1$, where $\vec{z}_k^m$ is the average of the neighbouring nodes of $\vec{q}_k^m$. Of course, (i) with $\alpha = 0$ is equivalent to using (2.4) in place of (2.17a,b). Unless otherwise stated, we will always choose strategy (i) in this paper, with $\alpha = 0$ if not stated otherwise.

An alternative to trying to influence the tangential movement of vertices within the framework of the evolution equations, as discussed above, is to do a separate redistribution step after each time step. Here we recall ideas described in Barrett, Garcke, and Nürnberg (2006, Remark 2.7), where a scheme based on the "evolution equation" $\mathcal{V} = 0$ was introduced in order to produce good triangulations of given surfaces. Here we extend this idea to incorporate tangential forces as described above. In particular, we introduce the scheme: Find $\{\vec{X}^{m+1}, \kappa^{m+1}\} \in \underline{V}(\Gamma^m) \times V(\Gamma^m)$ such that

$$\langle \frac{\vec{X}^{m+1} - \vec{X}^m}{\tau_m}, \chi\, \vec{\nu}^m \rangle_m^h = 0, \qquad \forall\ \chi \in W(\Gamma^m), \tag{2.20}$$

and (2.17a,c) hold. In practice, this redistribution procedure worked well for the strategy (2.19)(*iii*), i.e. when the tangential components of $\frac{\vec{X}^{m+1}-\vec{X}^m}{\tau_m}$ are given explicitly. In practice, for certain complicated flows, e.g. the higher genus experiments in Section 4, we will use (2.20) with (2.19)(*iii*) as a "heuristical" redistribution step, similarly to the strategies described in Brakke (1992) and Bänsch, Morin, and Nochetto (2005). Then one step of (2.20) will be applied after each basic evolution step in order to prevent undesirable mesh formations. From now on when we refer to (2.20), we mean the scheme (2.20), (2.17a,b) with strategy (2.19)(*iii*).

3 Solution of the algebraic equations

3.1 Willmore and Helfrich flow

First we show existence and uniqueness for the solutions to our schemes discussed in the previous section.

THEOREM. 3.1. *Let the assumption* ($\mathcal{A}$) *hold. Then there exists a unique solution* $\{\vec{X}^{m+1}, \kappa^{m+1}\} \in \underline{V}(\Gamma^m) \times V(\Gamma^m)$ *to the systems* (2.5), (2.6)*;* (2.7) *and* (2.8) *together with either* (2.4) *or* (2.17a,b) *with* (2.19)(*i*) *with* $\alpha > 0$ *or* (*ii*)*. In the latter two cases, the solutions* $\beta_i^{m+1} \in V(\Gamma^m)$, $i = 1 \to d-1$, *are also unique.*

Proof. We first discuss (2.5), (2.6) with (2.17a,b). Existence and uniqueness of $\underline{\underline{W}} \in \underline{\underline{V}}(\Gamma^m)$ that solves (2.5) is obvious. Then (2.6) is a linear system, so existence follows from uniqueness. To investigate the latter, we consider the system: Find $\{\vec{X}, \kappa, \beta_1, \ldots, \beta_{d-1}\} \in \underline{V}(\Gamma^m) \times [V(\Gamma^m)]^d$ such that

$$\langle \vec{X}, \chi\, \vec{\nu}^m \rangle_m^h - \tau_m \, \langle \nabla_s \kappa, \nabla_s \chi \rangle_m - \tfrac{1}{2}\, \tau_m \, \langle (\kappa^m - \overline{\varkappa})^2 \, \kappa, \chi \rangle_m^h = 0 \qquad \forall\ \chi \in V(\Gamma^m), \quad (3.1a)$$

$$\langle \alpha_i^m \, \vec{X}, \chi\, \vec{\tau}_i^m \rangle_m^h - \tau_m \, \langle \alpha_i^m \, \delta_i^m \, \beta_i, \chi \rangle_m^h = 0, \quad i = 1 \to d-1, \qquad \forall\ \chi \in V(\Gamma^m), \quad (3.1b)$$

$$\langle \kappa\, \vec{\omega}^m + \sum_{i=1}^{d-1} \alpha_i^m \, \beta_i \, \vec{\tau}_i^m, \vec{\eta} \rangle_m^h + \langle \nabla_s \vec{X}, \nabla_s \vec{\eta} \rangle_m = 0 \qquad \forall\ \vec{\eta} \in \underline{V}(\Gamma^m). \quad (3.1c)$$

Choosing $\chi \equiv \kappa \in V(\Gamma^m)$ in (3.1a), $\chi \equiv \beta_i \in V(\Gamma^m)$ in (3.1b) for $i = 1 \to d-1$, and $\vec{\eta} \equiv \vec{X} \in \underline{V}(\Gamma^m)$ in (3.1c) yields on combining that

$$|\nabla_s \vec{X}|_m^2 + \tau_m \, |\nabla_s \kappa|_m^2 + \tau_m \sum_{i=1}^{d-1} \langle \alpha_i^m \, \delta_i^m \, \beta_i, \beta_i \rangle_m^h + \tfrac{1}{2}\, \tau_m \, |(\kappa^m - \overline{\varkappa})\, \kappa|_{m,h}^2 = 0\,. \quad (3.2)$$

It follows from (3.2) that $\kappa \equiv \kappa^c \in \mathbb{R}$ and $\vec{X} \equiv \vec{X}^c \in \mathbb{R}^d$; and hence, on noting that $\alpha_i^m \, \delta_i^m > 0$, $i = 1 \to d-1$, that

$$\langle \vec{X}^c, \chi\, \vec{\nu}^m \rangle_m^h = 0 \quad \forall\ \chi \in V(\Gamma^m), \qquad \kappa^c \, \langle \vec{\nu}^m, \vec{\eta} \rangle_m^h = 0 \quad \forall\ \vec{\eta} \in \underline{V}(\Gamma^m)\,. \quad (3.3)$$

Choosing $\vec{\eta} \equiv \vec{z}\,\phi_k^m \in \underline{V}(\Gamma^m)$ in (3.3), and noting (2.1) and (2.2), yields, on assuming $\kappa^c \neq 0$, that for $k = 1 \to K$

$$\vec{\omega}_k^m \,.\, \vec{z} = 0 \quad \forall\ \vec{z} \in \mathbb{R}^d \qquad \Longleftrightarrow \qquad \vec{\omega}_k^m = \vec{0}\,. \tag{3.4}$$

However, this contradicts assumption $(\mathcal{A})$ and hence $\kappa^c = 0$. Similarly, choosing $\chi \equiv \phi_k^m$ in (3.3) yields that $\vec{X}^c \,.\, \vec{\omega}_k^m = 0$ for $k = 1 \to K$. It follows from assumption $(\mathcal{A})$ that $\vec{X}^c \equiv \vec{0}$. Hence we have shown that there exists a unique solution $\{\vec{X}^{m+1}, \kappa^{m+1}\} \in \underline{V}(\Gamma^m) \times V(\Gamma^m)$ to (2.6) with (2.17a,b). The uniqueness result for β_i^m, $i = 1 \to d-1$, follows immediately from (3.2). The same result for (2.6), (2.4) is just the special case $\alpha_i^m \equiv 0$, $i = 1 \to d-1$. The given proof naturally extends to all the other schemes as well. □

Here and throughout, for a given $n \in \mathbb{N}$, let $\vec{Id}_n \in (\mathbb{R}^{d\times d})^{n\times n}$ be the identity matrix, and similarly for $Id_n \in \mathbb{R}^{n\times n}$. We introduce also the matrices $\vec{N}_m \in (\mathbb{R}^d)^{K\times K}$, $A_m \in \mathbb{R}^{K\times K}$ and $\vec{A}_m \in (\mathbb{R}^{d\times d})^{K\times K}$ with entries

$$[\vec{N}_m]_{kl} := \int_{\Gamma^m} \pi_m^h[\phi_k\,\phi_l]\,\vec{\nu}^m \,\mathrm{d}s, \quad [A_m]_{kl} := \langle \nabla_s\phi_k, \nabla_s\phi_l\rangle_m, \quad [\vec{A}_m]_{kl} := [A_0]_{kl}\,\vec{Id}_1\,, \tag{3.5}$$

where $\pi_m^h : C(\Gamma^m, \mathbb{R}) \to V(\Gamma^m)$ is the standard interpolation operator at the nodes $\{\vec{q}_k^m\}_{k=1}^K$.

Similarly to (3.5), we introduce the matrix $M_m \in \mathbb{R}^{K\times K}$ by

$$[M_m]_{kl} := \langle ([\lambda^m]_+ + \tfrac{1}{2}\,(\kappa^m - \overline{\varkappa})^2)\,\phi_k, \phi_l\rangle_m^h\,,$$

and then rewrite (2.5), (2.6) and (2.7) in terms of

$$\begin{pmatrix} \tau_m\,(A_m + M_m) & -\vec{N}_m^T \\ \vec{N}_m & \vec{A}_m \end{pmatrix} \begin{pmatrix} \kappa^{m+1} \\ \delta\vec{X}^{m+1} \end{pmatrix} = \begin{pmatrix} b \\ -\vec{A}_m\,\vec{X}^m \end{pmatrix}, \tag{3.6}$$

where $b \in \mathbb{R}^K$ with $b_k = \tau_m\,\langle(\kappa^m - \overline{\varkappa})\,|\underline{\underline{W}}^m|^2, \phi_k\rangle_m^h$, $k = 1 \to K$, or $b_k = \tau_m\,\langle(\kappa^m - \overline{\varkappa})\,|\nabla_s\,\vec{v}^m|^2, \phi_k\rangle_m^h$, $k = 1 \to K$, respectively.

The solution to (3.6) can be found as follows. On assuming that $\kappa^m \not\equiv \overline{\varkappa}$, the matrix $\widehat{A}_m := A_m + M_m$ is positive definite and we can solve (3.6) by solving the Schur complement

$$(\vec{A}_m + \tfrac{1}{\tau_m}\,\vec{N}_m\,\widehat{A}_m^{-1}\,\vec{N}_m^T)\,\delta\vec{X}^{m+1} = -\vec{A}_m\,\vec{X}^m - \tfrac{1}{\tau_m}\vec{N}_m\,\widehat{A}_m^{-1}\,b\,, \tag{3.7}$$

and then setting

$$\kappa^{m+1} = \tfrac{1}{\tau_m}\,\widehat{A}_m^{-1}\,[\vec{N}_m^T\,\delta\vec{X}^{m+1} + b]\,. \tag{3.8}$$

In the case that $\kappa^m \equiv \overline{\varkappa}$ and $\lambda^m < 0$, the matrix $\widehat{A}_m$ has the nontrivial kernel $\mathrm{span}\{1\}$, where $1 := (1, \ldots, 1)^T \in \mathbb{R}^K$. Then, similarly to the techniques used in Barrett, Garcke, and Nürnberg (2006), one needs to introduce the inverse S_m of $\widehat{A}_m$ restricted on the set $(\mathrm{span}\{1\})^\perp$ and adapt (3.7), (3.8) accordingly. However, the case $\kappa^m \equiv \overline{\varkappa}$ never occurred in practice.

We note that the Schur complement system (3.7) can be easily solved with a conjugate gradient solver. The scheme (2.8), and all the variants involving (2.17a,b) can be solved in a very similar fashion. Finally, the solution to (2.20) with (2.17a,b) and (2.19)(iii) is given by $\vec{X}^{m+1}(\vec{q}_k^m) = \vec{X}^m(\vec{q}_k^m) + \sum_{i=1}^{d-1}[(\vec{z}_k^m - \vec{q}_k^m)\,.\,\vec{\tau}_{i,k}^m]\,\vec{\tau}_{i,k}^m$.

3.2 Gauß curvature flow

Clearly, the scheme (2.9) is a special case of

$$\langle \frac{\vec{X}^{m+1}-\vec{X}^m}{\tau_m}, \chi\, \vec{\nu}^m \rangle_m^h = \langle g^m, \chi \rangle_m^h \,, \tag{3.9}$$

where $g^m \in V(\Gamma^m)$ is given. The solution of (3.9), (2.4), which in matrix form can be written as

$$\begin{pmatrix} 0 & \frac{1}{\tau_m}\vec{N}_m^T \\ \vec{N}_m & \vec{A}_m \end{pmatrix} \begin{pmatrix} \kappa^{m+1} \\ \delta\vec{X}^{m+1} \end{pmatrix} = \begin{pmatrix} M_m\, g^m \\ -\vec{A}_m \vec{X}^m \end{pmatrix}, \tag{3.10}$$

is straightforward, on writing $\delta\vec{X}^{m+1} = \vec{N}_m\, y_0 + \sum_{i=1}^2 \vec{N}_{m,i}^{\perp}\, y_i$, where $y_i \in \mathbb{R}^K$, $i = 0 \to 2$, and where we recall that here $d = 3$. The diagonal matrices $\vec{N}_{m,i}^{\perp} \in (\mathbb{R}^d)^{K\times K}$ are given by their diagonal entries $[\vec{N}_{m,i}^{\perp}]_{kk} = \langle \phi_k^m, \phi_k^m \rangle_m^h\, \vec{\tau}_{i,k}^m$, where we recall the notation from Section 2.4. Then we immediately obtain that

$$y_0 = \tau_m\, (\vec{N}_m^T\, \vec{N}_m)^{-1}\, M_m\, g^m \,, \tag{3.11}$$

with (y_1, y_2) being the unique solution of the symmetric linear system

$$\begin{pmatrix} (\vec{N}_{m,1}^{\perp})^T \vec{A}_m \vec{N}_{m,1}^{\perp} & (\vec{N}_{m,1}^{\perp})^T \vec{A}_m \vec{N}_{m,2}^{\perp} \\ (\vec{N}_{m,2}^{\perp})^T \vec{A}_m \vec{N}_{m,1}^{\perp} & (\vec{N}_{m,2}^{\perp})^T \vec{A}_m \vec{N}_{m,2}^{\perp} \end{pmatrix} \begin{pmatrix} y_1 \\ y_2 \end{pmatrix} = - \begin{pmatrix} (\vec{N}_{m,1}^{\perp})^T \vec{A}_m \vec{X}^m + (\vec{N}_{m,1}^{\perp})^T \vec{A}_m \vec{N}_m\, y_0 \\ (\vec{N}_{m,2}^{\perp})^T \vec{A}_m \vec{X}^m + (\vec{N}_{m,2}^{\perp})^T \vec{A}_m \vec{N}_m\, y_0 \end{pmatrix}.$$

4 Numerical results

In this section we present several numerical computations. Unless otherwise stated, we will always use the scheme (2.7) for the Willmore flow simulations. In addition, we always use $\overline{\varkappa} = \varrho = 0$, unless stated otherwise.

Throughout this section we use (almost) uniform time steps; in that, $\tau_m = \tau$, $m = 0 \to M-2$, and $\tau_{M-1} = T - t_{m-1} \leq \tau$. For later purposes, we define

$$\vec{X}(\cdot,t) := \tfrac{t-t_{m-1}}{\tau_{m-1}}\, \vec{X}^m(\cdot) + \tfrac{t_m - t}{\tau_{m-1}}\, \vec{X}^{m-1}(\cdot) \qquad t \in [t_{m-1}, t_m] \quad m \geq 1. \tag{4.1}$$

On recalling (2.2), we set $h_{\vec{X}^m} := \max_{k=1\to K} \Big\{ \max_{\vec{p}_l \in \partial\Lambda_k^m} |\vec{X}^m(\vec{q}_k^m) - \vec{X}^m(\vec{p}_l)| \Big\}$.

We recall that all of our schemes in Section 2 need an initial value κ^0 for the approximation of mean curvature. It turns out that this choice is critically important for the accuracy of the numerical approximation, and in particular for the volume and surface area preservation properties of our schemes for e.g. Helfrich flow. In the case $d = 2$ and on noting that $\vec{N}_0^{\,T}\, \vec{N}_0$ is a diagonal matrix with strictly positive diagonal entries, we use as initial data

$$\kappa^0 := -(\vec{N}_0^{\,T}\, \vec{N}_0)^{-1} \vec{N}_0^{\,T}\, \vec{A}_0\, \vec{X}^0. \tag{4.2}$$

However, for $d = 3$ this choice is no longer appropriate. In this case, on noting (1.1), we consider the following choice

$$\langle \kappa^0, \chi \rangle_0^h = -\langle \mathrm{tr}(\nabla_s \vec{\nu}^0), \chi \rangle_0^h \qquad \forall\, \chi \in V(\Gamma^0)\,, \tag{4.3}$$

where we recall (2.3). For later use we also define the discrete curvature vector $\vec{\kappa}^0 \in \underline{V}(\Gamma^0)$ such that

$$\langle \vec{\kappa}^0, \vec{\eta} \rangle_0^h = -\langle \nabla_s \vec{X}^0, \nabla_s \vec{\eta} \rangle_0 \qquad \forall\, \vec{\eta} \in \underline{V}(\Gamma^0)\,, \tag{4.4}$$

which was e.g. used in Hsu, Kusner, and Sullivan (1992) in order to define the discrete Willmore energy of Γ^0 by

$$E_0^0 := \tfrac{1}{2}\, \langle \vec{\kappa}^0, \vec{\kappa}^0 \rangle_0^h. \tag{4.5}$$

A small improvement on this was suggested in Sullivan (2002), where $\vec{\kappa}^0$ in (4.5) is replaced by $\tilde{\kappa}^0 \in \underline{V}(\Gamma^0)$ such that

$$\tilde{\kappa}^0(\vec{q}_k^0) := \frac{1}{|\vec{\omega}_k^0|}\, \vec{\kappa}^0(\vec{q}_k^0)\,, \qquad k = 1 \to K\,. \tag{4.6}$$

For any errors displayed in the tables below, we will always compute e.g. the distance $\|\vec{X} - \vec{x}\|_{L^\infty} := \max_{m=1\to M} \|\vec{X}(\cdot,t_m) - \vec{x}(\cdot,t_m)\|_{L^\infty}$, where $\|\vec{X}(\cdot,t_m) - \vec{x}(\cdot,t_m)\|_{L^\infty} := \max_{k=1\to K} |\vec{X}^m(\vec{q}_k^m) - \vec{q}_k^{m,\star}|$, between $\vec{X}$ and the true solution $\vec{x}$ on the interval $[0,T]$, where $\vec{q}_k^{m,\star}$ is the orthogonal projection of $\vec{q}_k^m \equiv \vec{X}^m(\vec{q}_k^m)$ onto the true surface $\Gamma(t_m)$ parameterized by $\vec{x}(\cdot,t_m)$. This norm is naturally extended to a scalar-, vector-, or matrix-valued quantity u defined on $\Gamma(\cdot)$ and its approximation U, where U is a piecewise linear in time interpolation of U^m, $m = 0 \to M$, similarly to (4.1). In addition, we define e.g. the norm $\|U - u\|_{L^\infty(L^2)} := \max_{m=1\to M} \|U^m(\cdot) - u(\cdot,t_m)\|_{L^2}$, where $\|U^m(\cdot) - u(\cdot,t_m)\|_{L^2} := (\sum_{k=1}^K \langle \phi_k^m, \phi_k^m \rangle_m^h\, |U^m(\vec{q}_k^m) - u(\vec{q}_k^{m,\star}, t_m)|^2)^{\frac{1}{2}}$.

Finally, we note that we implemented the approximations within the finite element toolbox ALBERTA, see Schmidt and Siebert (2005).

4.1 Results for $d = 2$

4.1.1 Willmore flow

At first we perform a convergence test for our two approximations (2.5), (2.6) and (2.7) and compare the results with the following scheme from Barrett, Garcke, and Nürnberg (2007) for the Willmore flow of curves: Find $\{\vec{X}^{m+1}, \kappa^{m+1}\} \in \underline{V}(\Gamma^m) \times V(\Gamma^m)$ such that

$$\langle \frac{\vec{X}^{m+1} - \vec{X}^m}{\tau_m}, \chi\, \vec{\nu}^m \rangle_m^h - \langle \nabla_s\, \kappa^{m+1}, \nabla_s\, \chi \rangle_m = -\tfrac{1}{2}\, \langle (\kappa^m)^3, \chi \rangle_m^h \qquad \forall\, \chi \in V(\Gamma^m), \tag{4.7}$$

and (2.4) hold.

	(4.7)		(2.5), (2.6)		(2.7)	
K	$\|\vec{X}-\vec{x}\|_{L^\infty}$	$\|\kappa-\varkappa\|_{L^\infty}$	$\|\vec{X}-\vec{x}\|_{L^\infty}$	$\|\kappa-\varkappa\|_{L^\infty}$	$\|\vec{X}-\vec{x}\|_{L^\infty}$	$\|\kappa-\varkappa\|_{L^\infty}$
10	2.2124e-01	2.4442e-01	7.3025e-02	2.3171e-01	2.9794e-02	2.1455e-01
20	3.6298e-02	6.0862e-02	1.5618e-02	6.0203e-02	5.3336e-03	5.9121e-02
40	8.5412e-03	1.5331e-02	3.8660e-03	1.5292e-02	1.5240e-03	1.5225e-02
80	2.1143e-03	3.8504e-03	9.7480e-04	3.8480e-03	3.9623e-04	3.8438e-03
160	5.2844e-04	9.6493e-04	2.4558e-04	9.6478e-04	1.0046e-04	9.6452e-04
320	1.3224e-04	2.4153e-04	6.1681e-05	2.4152e-04	2.5257e-05	2.4150e-04
640	3.3086e-05	6.0421e-05	1.5460e-05	6.0418e-05	6.3300e-06	6.0419e-05

Table 1: Absolute errors $\|\vec{X}-\vec{x}\|_{L^\infty}$ and $\|\kappa-\varkappa\|_{L^\infty}$ for the test problem.

An exact solution to (1.10), see Barrett, Garcke, and Nürnberg (2007, p. 460), is given by

$$\vec{x}(\rho,t) = (1+2\,t)^{\frac{1}{4}}\,(\cos g(\rho), \sin g(\rho))^T, \quad \varkappa(\rho,t) = -(1+2\,t)^{-\frac{1}{4}}, \tag{4.8}$$

where for ease of notation we parameterize $\Gamma(t)$ over the interval $[0,1] \subset \mathbb{R}$, and where $g(\rho) = 2\pi\rho + 0.1\,\sin(2\pi\rho)$ in order to make the initial distribution of nodes non-uniform. The results can be seen in Table 1, where we report on the errors $\|\vec{X}-\vec{x}\|_{L^\infty}$ and $\|\kappa-\varkappa\|_{L^\infty}$ for $T=1$ and $\tau = 0.5\,h^2$. The reported values indicate that these quantities converge with order $O(h^2)$ for all three schemes, while the approximation (2.7) exhibits the smallest absolute errors.

4.1.2 Helfrich flow

We performed the following experiments for the scheme (2.8) for initially elongated tubes of total dimensions 4×1, 8×1 and 12×1. The discretization parameters were $K = J = 128$ and $\tau = 10^{-4}$. See Figure 1 for the results, where we observe that only in the latter case does the steady state shape exhibit self intersections. Note that the experiments have reached a numerical steady state at times $T=1$, $T=2$ and $T=5$, respectively, where the relative losses in length and area were -0.09% and -0.002%, -0.03% and -0.003% and -0.02% and -0.003%, respectively.

4.2 Results for $d = 3$

4.2.1 Experimental convergence tests

Before we report on numerical simulations for the geometric evolution equations considered in this paper, we investigate experimentally the quality of possible discretizations of certain geometric quantities of a given surface.

We start with possible ways to extract discrete mean curvature values from a given

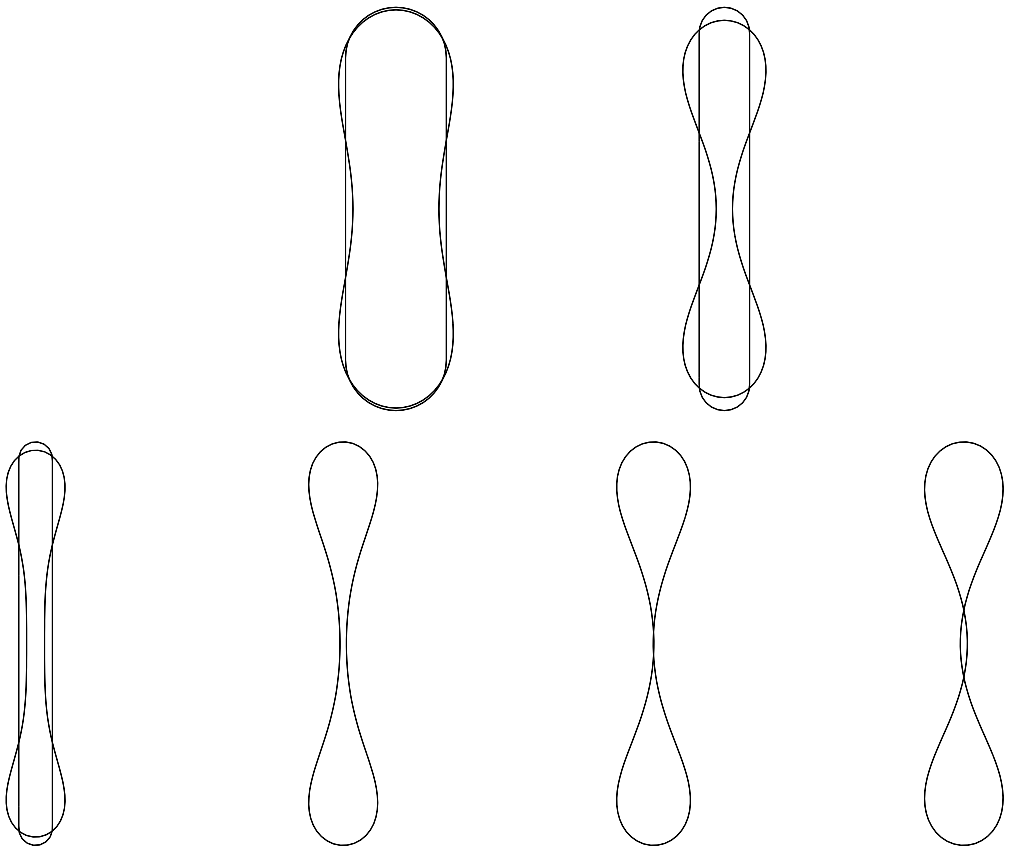

Figure 1: Helfrich flow for elongated tubes. $\vec{X}(t)$ for $t = 0,\ 1$ (top left), $\vec{X}(t)$ for $t = 0,\ 2$ (top right) and $\vec{X}(t)$ for $t = 0,\ 1,\ 2,\ 3,\ 5$ (bottom).

polyhedral surface. Here we compare the approaches (4.2), (4.6) and (4.3) for a unit sphere (see Table 2) and for a Clifford torus, i.e. a torus with large radius $R = \sqrt{2}$ and small radius $r = 1$, (see Table 5). In addition, we performed tests where we integrate one step of our Willmore flow scheme (2.7) for different choices of κ^0 and report on the L^∞ error for the discrete curvature κ^1. See Table 3 for the results for the unit sphere and Table 6 for a Clifford torus. In each case we chose $\tau = 0.125\, h^2_{\vec{X}^0}$.

Similarly, we report on tables for possible approximations of the Gauß curvature, see Table 4 (for the unit sphere) and Table 7 (for a Clifford torus).

What all of these convergence tests appear to show is that firstly, the discrete curvature values κ^m computed from our approximation (2.7), say, exhibit good convergence properties in L^∞ (compare Tables 3 and 6). And secondly, discrete geometric quantities based on the approximation $\nabla_s \vec{v}^m$ of the Weingarten map $\underline{\underline{w}} = \nabla_s \vec{\nu}$, converged for the surfaces considered here in L^2, but not in L^∞. All the other discrete approximations, including (2.5), never converged. We note that the latter confirms observations reported in Heine (2007) for linear finite elements, whereas convergence in L^2 is proved there for higher order elements. We note that replacing the discrete vertex normals $\vec{v}^m$ with a discrete normal $\vec{\nu}^h$ that is obtained by locally fitting vertices to a biquadratic surface,

		(4.3)		(4.2)		(4.6)	
K	$h_{\vec{X}^0}$	L^∞	L^2	L^∞	L^2	L^∞	L^2
50	7.6537e-01	4.4409e-16	1.1291e-15	1.1559e-00	2.6103e-00	1.1567e-00	2.6116e-00
194	4.0994e-01	1.0321e-01	1.4140e-01	1.2583e-00	2.8490e-00	1.2587e-00	2.8482e-00
770	2.0854e-01	1.3436e-01	8.5989e-02	1.2925e-00	2.9137e-00	1.2926e-00	2.9135e-00
3074	1.0472e-01	1.4227e-01	4.5485e-02	1.3017e-00	2.9309e-00	1.3018e-00	2.9308e-00
12290	5.2416e-02	1.4425e-01	2.3677e-02	1.3041e-00	2.9355e-00	1.3041e-00	2.9355e-00
49154	2.6215e-02	1.4475e-01	1.2552e-02	1.3047e-00	2.9369e-00	1.3047e-00	2.9369e-00
196610	1.3108e-02	1.4487e-01	6.9159e-03	1.3048e-00	2.9373e-00	1.3048e-00	2.9373e-00

Table 2: L^∞ and L^2 errors for the discrete curvatures κ^0 for a sphere.

K	$h_{\vec{X}^0}$	(4.3)	(4.2)	(4.6)
50	7.6537e-01	1.0097e-01	6.7826e-02	6.7983e-02
194	4.0994e-01	3.3421e-02	3.0081e-02	3.0114e-02
770	2.0854e-01	1.2860e-02	1.0169e-02	1.0174e-02
3074	1.0472e-01	6.2023e-03	2.0763e-03	2.0762e-03
12290	5.2416e-02	3.1184e-03	1.2355e-03	1.2354e-03
49154	2.6215e-02	1.5930e-03	1.0917e-03	1.0917e-03
196610	1.3108e-02	8.1239e-04	6.6861e-04	6.6861e-04

Table 3: L^∞ errors for the discrete curvature κ^1 for a sphere.

similarly to the technique described in Meek and Walton (2000), it is possible to obtain $O(h)$ convergence in L^∞ for the corresponding mean and Gauß curvature definitions based on $\nabla_s \vec{\nu}^h$. However, this method did not prove robust in practice for the geometric evolution equations considered here, and so we do not employ it in this paper.

In order to underline the good properties of $\nabla_s \vec{v}^m$, we now test this quantity for the evolution of a sphere under mean curvature flow, where the true solutions $\vec{x}$ and $\underline{\underline{w}}$ are readily available. To this end, we start the evolution with very non-uniform triangulations of the unit sphere, as depicted in Figure 2, and then monitor the error between the discrete Weingarten maps $\nabla_s \vec{v}(\cdot, t_m)$ and the true $\underline{\underline{w}}(\cdot, t_m)$; see Table 8 for the results.

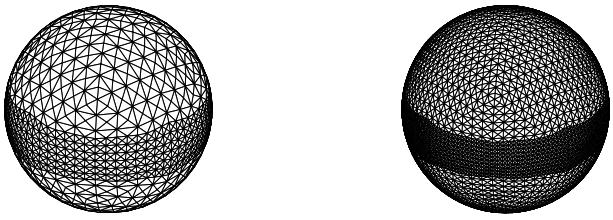

Figure 2: Non-uniform triangulations of the unit sphere for $K = 1378$ and $K = 5058$.

K	$h_{\vec{X}^0}$	(2.10)	(2.11)	(2.12)
50	7.6537e-01	1.1920e-15	3.5911e-00	1.3208e-00
194	4.0994e-01	1.3740e-01	4.4261e-00	1.4286e-00
770	2.0854e-01	8.4805e-02	4.7312e-00	1.4580e-00
3074	1.0472e-01	4.5480e-02	4.8354e-00	1.4657e-00
12290	5.2416e-02	2.4043e-02	4.8729e-00	1.4678e-00
49154	2.6215e-02	1.3012e-02	4.8877e-00	1.4685e-00
196610	1.3108e-02	7.3662e-03	4.8941e-00	1.4687e-00

Table 4: L^2 errors for $\mathcal{K}^0$ for a sphere. For (2.11) we used $\kappa^0 = \pi^0 \varkappa$ in (2.5).

		(4.3)		(4.2)		(4.6)	
K	$h_{\vec{X}^0}$	L^∞	L^2	L^∞	L^2	L^∞	L^2
32	1.9734e-00	2.0449e-00	4.8132e-00	1.2753e-00	5.4045e-00	1.7662e-00	6.3337e-00
128	1.1352e-00	1.1446e-00	1.8404e-00	7.9422e-01	3.4854e-00	2.9714e-00	5.2819e-00
512	5.8945e-01	4.7048e-01	5.3457e-01	7.1780e-01	3.1482e-00	3.3635e-00	5.0069e-00
2048	3.6083e-01	5.4515e-02	1.2913e-01	7.1448e-01	3.1455e-00	3.5273e-00	5.0526e-00
8192	1.8165e-01	1.3734e-02	3.2915e-02	7.0894e-01	3.1424e-00	3.5335e-00	5.0587e-00
32768	7.4729e-02	9.5999e-03	9.1629e-03	7.0727e-01	3.1398e-00	3.5326e-00	5.0566e-00
131072	3.7371e-02	2.4209e-03	2.2974e-03	7.0715e-01	3.1411e-00	3.5348e-00	5.0597e-00

Table 5: L^∞ and L^2 errors for κ^0 for a Clifford torus.

Here $(\nabla_s \vec{v})(\cdot, t_m) \in \underline{\underline{V}}(\Gamma^m)$ is given by

$$\langle (\nabla_s \vec{v})(\cdot, t_m), \underline{\underline{\chi}} \rangle_m^h = \langle \nabla_s \vec{v}^m, \underline{\underline{\chi}} \rangle_m^h \qquad \forall\ \underline{\underline{\chi}} \in \underline{\underline{V}}(\Gamma^m)\,,$$

and we set $T = 0.125$ and used $\tau = \tau = 0.125\, h^2_{\vec{X}^0}$. The results in Table 8 appear to show that in the norm $L^\infty(L^2)$, the approximation $\nabla_s \vec{v}$ does converge as $h \to 0$.

4.2.2 Gauß curvature flow

We start with a convergence experiment for our scheme (2.9), which represents another test for our approximation $\nabla_s \vec{v}$ of the Weingarten map. An exact solution to (1.16) with $\theta(\vec{\nu}) = 1$ is a sphere of radius $(1 - (2\,\rho + 1)\, t)^{\frac{1}{2\,\rho+1}}$, for $t \in [0, \overline{T})$ with extinction time $\overline{T} = \frac{1}{2\,\rho+1}$. We compare our results from (2.9) to this exact solution for $\rho = 1$ and $\rho = \frac{1}{4}$, see Table 9. We used very non-uniform initial triangulations for the unit sphere, see Figure 2, and used $\tau = 0.01\, h^2_{\vec{X}^0}$ with either $T = \frac{1}{2}\,\overline{T}$ or $T = 0.9\,\overline{T}$. These results underline once more, that in practice the discrete Weingarten map $\nabla_s \vec{v}$ works well.

The same computations for the scheme (2.13) can be seen in Table 10. We observe that the approximation (2.13) did not always manage to integrate to the final time T. This is due to developing instabilities, especially closer to the singularity time $\overline{T}$. It is

K	$h_{\vec{X}^0}$	(4.3)	(4.2)	(4.6)
32	1.9734e-00	2.3541e-00	1.7370e-00	3.3879e-00
128	1.1352e-00	8.5952e-01	5.5560e-01	3.0342e-00
512	5.8945e-01	2.5202e-01	2.0873e-01	1.9279e-00
2048	3.6083e-01	2.5925e-02	2.2230e-02	1.2648e-00
8192	1.8165e-01	4.5312e-03	7.4613e-03	5.7053e-01
32768	7.4729e-02	3.0723e-03	4.2878e-03	1.5785e-01
131072	3.7371e-02	8.0550e-04	1.2713e-03	4.8671e-02

Table 6: L^∞ errors for κ^1 for a Clifford torus.

K	$h_{\vec{X}^0}$	(2.10)	(2.11)	(2.12)
32	1.9734e-00	4.3051e-00	7.7576e-00	4.0465e-00
128	1.1352e-00	1.7908e-00	6.1834e-00	2.3208e-00
512	5.8945e-01	5.8285e-01	5.3685e-00	1.6509e-00
2048	3.6083e-01	6.0269e-02	5.5146e-00	1.7165e-00
8192	1.8165e-01	1.5342e-02	5.6887e-00	1.7042e-00
32768	7.4729e-02	1.1720e-02	5.7391e-00	1.6977e-00
131072	3.7371e-02	2.9389e-03	5.7518e-00	1.6996e-00

Table 7: L^2 errors for $\mathcal{K}^0$ for a Clifford torus. For (2.11) we used $\kappa^0 = \pi^0 \varkappa$ in (2.5).

K	$h_{\vec{X}^0}$	$\|\vec{X} - \vec{x}\|_{L^\infty}$	$\|\nabla_s \vec{v} - \underline{\underline{w}}\|_{L^\infty}$	$\|\nabla_s \vec{v} - \underline{\underline{w}}\|_{L^\infty(L^2)}$
106	7.6537e-01	5.5049e-02	7.8696e-01	1.9719e-00
402	4.0994e-01	2.3865e-02	5.3160e-01	9.8033e-01
1378	2.0854e-01	7.0417e-03	4.1083e-01	3.8731e-01
5058	1.0472e-01	1.8168e-03	4.3063e-01	2.6149e-01
20098	5.2416e-02	4.6757e-04	5.1682e-01	1.9002e-01
80130	2.6215e-02	1.1957e-04	5.2790e-01	1.3444e-01

Table 8: Absolute errors $\|\vec{X} - \vec{x}\|_{L^\infty}$, $\|\nabla_s \vec{v} - \underline{\underline{w}}\|_{L^\infty}$ and $\|\nabla_s \vec{v} - \underline{\underline{w}}\|_{L^\infty(L^2)}$ with $T = \frac{1}{8}$.

		$\rho = 1$		$\rho = \frac{1}{4}$	
K	$h_{\vec{X}^0}$	$T = \frac{1}{2}\overline{T}$	$T = 0.9\,\overline{T}$	$T = \frac{1}{2}\overline{T}$	$T = 0.9\,\overline{T}$
106	7.6537e-01	3.0994e-02	4.6174e-02	2.4148e-02	4.9160e-02
402	4.0994e-01	7.1883e-03	7.7524e-03	7.2118e-03	1.3296e-02
1378	2.0854e-01	3.0032e-03	3.0572e-03	2.3629e-03	3.3066e-03
5058	1.0472e-01	1.1509e-03	1.9247e-03	9.5111e-04	9.5111e-04
20098	5.2416e-02	5.2523e-04	1.3422e-03	2.7226e-04	2.7226e-04

Table 9: Absolute errors $\|\vec{X} - \vec{x}\|_{L^\infty}$ for the scheme (2.9) for $\rho = 1$ and $\rho = \frac{1}{4}$.

		$\rho = 1$		$\rho = \frac{1}{4}$	
K	$h_{\vec{X}^0}$	$T = \frac{1}{2}\overline{T}$	$T = 0.9\,\overline{T}$	$T = \frac{1}{2}\overline{T}$	$T = 0.9\,\overline{T}$
106	7.6537e-01	3.5866e-02	1.2577e-01	3.3105e-02	6.7034e-02
402	4.0994e-01	1.0053e-02	4.3964e-00	9.7216e-03	1.8711e-02
1378	2.0854e-01	2.6968e-03	–	2.4615e-03	5.0845e-03
5058	1.0472e-01	7.0309e-04	–	6.3529e-04	1.3311e-03
20098	5.2416e-02	1.8007e-04	–	1.6222e-04	3.3682e-04

Table 10: Absolute errors $\|\vec{X} - \vec{x}\|_{L^\infty}$ for the scheme (2.13) for $\rho = 1$ and $\rho = \frac{1}{4}$.

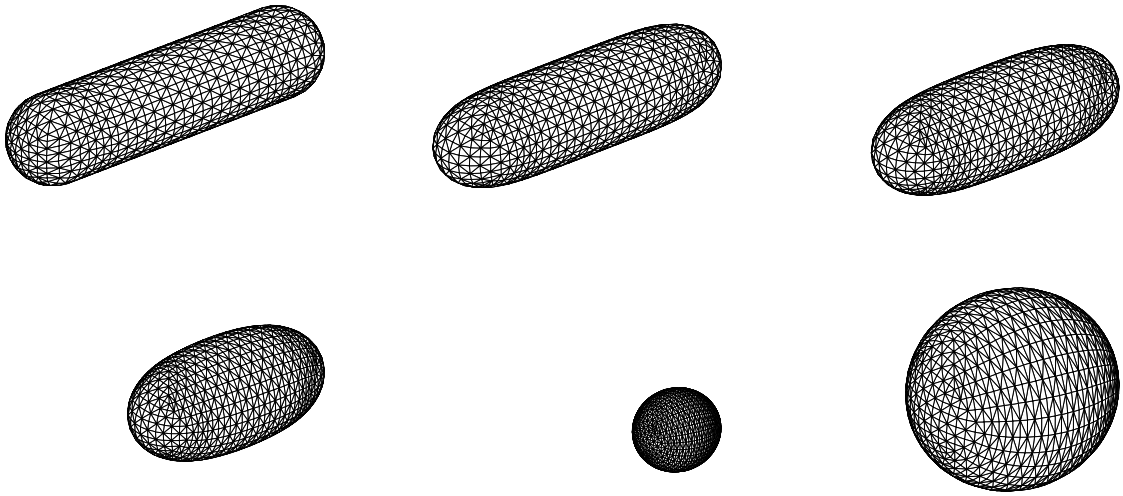

Figure 3: $\vec{X}(t)$ for $t = 0,\ 0.05,\ 0.1\,0.15,\ T = 0.22$ and $\vec{X}(T)$ (scaled).

likely that choosing sufficiently small time steps would enable also this scheme to compute the full evolution. We also note that the observed errors until $T = 0.9\,\overline{T}$ are always larger than for the scheme (2.9).

Next we compared the evolution of Gauß and mean curvature flow for a tubular shape of total dimensions $4 \times 1 \times 1$. The discretization parameters were $K = 1154$, $J = 2304$ and $\tau = 10^{-4}$, and the evolutions can be seen in Figures 3 and 4, respectively. We note that for the mean curvature flow experiment we used the scheme from Barrett, Garcke, and Nürnberg (2006). We observe that the cylindric part of the surface, where $\mathcal{K} = 0$ initially, is changed only very slowly for the Gauß curvature flow. Eventually the flow evolves the surface to a shrinking ball. The mean curvature flow, on the other hand, thins the cylindric part relatively quickly, so that the limiting shrinking shape resembles a needle.

In the literature, waiting time phenomena for the Gauß curvature flow are of interest, see e.g. Daskalopoulos and Hamilton (1999), Chopp, Evans, and Ishii (1999) and Daskalopoulos and Lee (2001). Here the initial surface exhibits some flat facets which

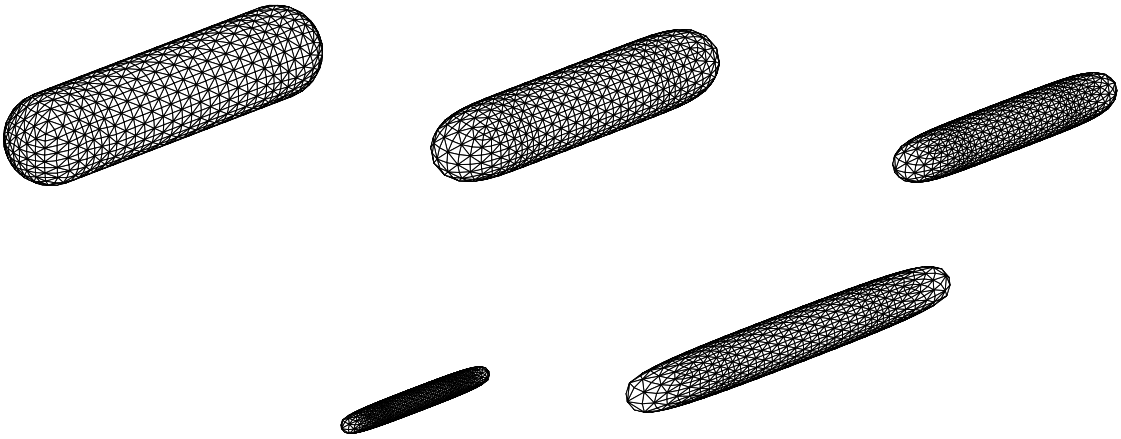

Figure 4: $\vec{X}(t)$ for $t = 0,\ 0.05,\ 0.1,\ T = 0.12$ and $\vec{X}(T)$ (scaled).

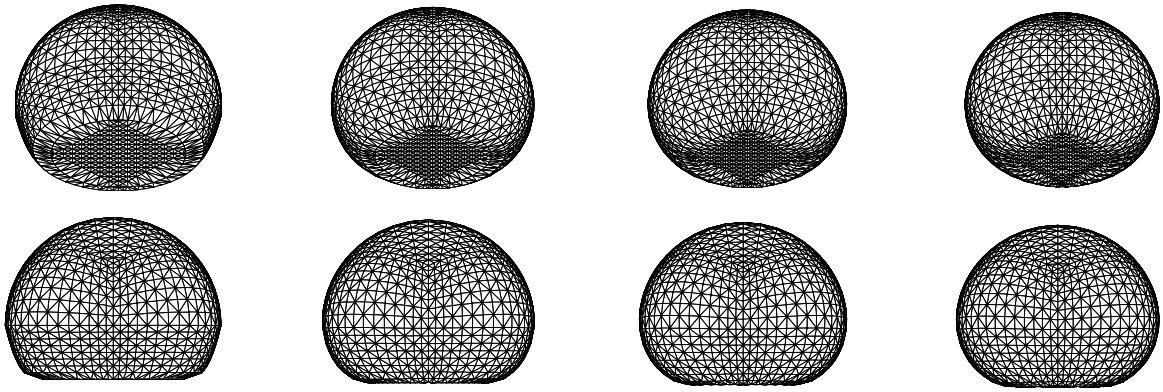

Figure 5: $\vec{X}(t)$ for $t = 0,\ 0.02,\ 0.04,\ 0.06$. Below a frontal view.

only start to move after some positive time t_0.

In order to investigate this numerically, we start with an initial surface that has a flat facet which connects smoothly to the rest of the surface. The discretization parameters are $K = 1538$, $J = 3072$, $\tau = 10^{-3}$, and the evolution can be seen in Figure 5. One can clearly observe that large parts of the flat facet of the initial surface remain unchanged at the beginning of the evolution, while e.g. the top of the surface moves slowly downwards.

4.2.3 Reduced/Induced tangential motion

We now conduct convergence experiments similar to Barrett, Garcke, and Nürnberg (2006), for the approximation (2.14) of mean curvature flow, together with (2.17a,b) and the possible strategies (2.19)(i) with $\alpha = 0.5$, (ii) with $\alpha = \delta = 1$ and (2.4) with one step of (2.20). The initial surface is a unit sphere and we used $T = 0.125$ and

K	$h_{\vec{X}^0}$	(i), $\alpha = 0$	(i), $\alpha = 0.5$	(ii), $\alpha = \delta = 1$	(2.4) with (2.20)
50	7.6537e-01	5.0141e-02	5.0320e-02	4.6513e-02	4.9628e-02
194	4.0994e-01	2.2436e-02	2.2944e-02	2.0353e-02	2.1308e-02
770	2.0854e-01	6.6398e-03	6.8145e-03	6.0021e-03	6.1807e-03
3074	1.0472e-01	1.7573e-03	1.8043e-03	1.5706e-03	1.6050e-03
12290	5.2416e-02	4.5446e-04	4.6646e-04	3.9965e-04	4.0684e-04
49154	2.6215e-02	1.1635e-04	1.1936e-04	1.0040e-04	1.0201e-04

Table 11: Absolute errors $\|\vec{X} - \vec{x}\|_{L^\infty}$ for the test problem, with $T = \frac{1}{8}$.

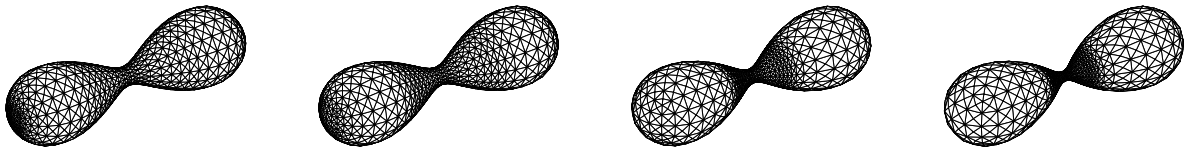

Figure 6: $\vec{X}(t)$ for $t = 0.24$ for $\alpha = 10^{-3}$, 5×10^{-4}, 10^{-4} and $\alpha = 0$.

$\tau = \tau = 0.125\, h^2_{\vec{X}^0}$; see Table 11 for the results. We see that all the schemes still converge with order $O(h^2)$. Of course, (2.19)(i) with $\alpha = 0$ just corresponds to the original scheme from Barrett, Garcke, and Nürnberg (2006). Hence we are satisfied that the tangential motion induced by (2.17a,b) has no influence on the accuracy of the approximations to geometric evolution equations considered in this paper. In the subsequent subsection, we will make regular use of the different strategies tested here.

An example of the effect of the scheme (2.17a,b) in practice can be seen in Figure 6, where we repeated an experiment for surface diffusion from Barrett, Garcke, and Nürnberg (2006) and compare the results for the strategy (2.19)(i) for different values of α. One can clearly observe the reduced tangential motion for $\alpha > 0$ compared to $\alpha = 0$.

4.2.4 Willmore flow

Often the Willmore flow is of interest, because stable stationary solutions of this flow are candidates for global minimizers of the Willmore energy, so-called Willmore surfaces. In this subsection, we will consider several evolutions that lead to such candidates. In order to get a better understanding of the quality of these approximations, we first investigate the performance of several discrete curvature definitions when being used to compute a discrete Willmore energy for a given polyhedral surface.

Starting with the unit sphere, we report on $\frac{1}{2}\langle \kappa^0, \kappa^0 \rangle^h_0$, where $\kappa^0 \in V(\Gamma^0)$ is defined by (4.2), (4.3) and (4.6), respectively. (Of course, in the latter case we report on the analogue of (4.5).) We do not report on values for (4.4), as they were very similar to

K	$h_{\vec{X}^0}$	$\mathrm{Vol}(0) - \frac{4}{3}\pi$	$\lvert\Gamma^0\rvert - 4\pi$	(4.3)	(4.2)	(4.6)
50	7.6537e-01	-5.1118e-01	-7.6967e-01	-1.5393e-00	5.0956e-00	5.1047e-00
194	4.0994e-01	-1.3816e-01	-1.9877e-01	-3.9402e-01	4.5258e-00	4.5338e-00
770	2.0854e-01	-3.5237e-02	-5.0096e-02	-9.7741e-02	4.3659e-00	4.3673e-00
3074	1.0472e-01	-8.8536e-03	-1.2549e-02	-2.4246e-02	4.3257e-00	4.3259e-00
12290	5.2416e-02	-2.2162e-03	-3.1389e-03	-6.0217e-03	4.3164e-00	4.3165e-00
49154	2.6215e-02	-5.5422e-04	-7.8482e-04	-1.4940e-03	4.3146e-00	4.3146e-00
196610	1.3108e-02	-1.3857e-04	-1.9621e-04	-3.6890e-04	4.3144e-00	4.3144e-00

Table 12: $\frac{1}{2}\langle\kappa^0,\kappa^0\rangle_0^h - 8\,\pi$.

K	$h_{\vec{X}^0}$	$\mathrm{Vol}(0) - \sqrt{8}\,\pi^2$	$\lvert\Gamma^0\rvert - \sqrt{32}\,\pi^2$	(4.3)	(4.2)	(4.6)
32	1.9734e-00	-1.1444e+01	-8.1193e-00	-9.0319e-00	2.6552e-00	2.7325e+01
128	1.1352e-00	-3.2254e-00	-1.7774e-00	-4.2114e-00	7.8555e-00	8.5186e-00
512	5.8945e-01	-8.3151e-01	-4.2452e-01	-1.4696e-00	5.1977e-00	5.4941e-00
2048	3.6083e-01	-2.9456e-01	-2.2503e-01	-6.2927e-01	5.2899e-00	5.2902e-00
8192	1.4920e-01	-5.2500e-02	-2.6741e-02	-1.0308e-01	4.9264e-00	4.9285e-00
32768	7.4729e-02	-1.3141e-02	-6.7342e-03	-2.5957e-02	4.9326e-00	4.9328e-00
131072	3.7371e-02	-3.2857e-03	-1.6844e-03	-6.5008e-03	4.9343e-00	4.9343e-00

Table 13: $\frac{1}{2}\langle\kappa^0,\kappa^0\rangle_0^h - 4\,\pi^2$.

the ones obtained for (4.6). The results are shown in Table 12. As can be seen, the choices (4.2) and (4.6) do not give reliable estimates for the true Willmore energy, while the definition (4.3) appears to converge to the true value as the discretization gets finer.

Next, we present a similar table for a so-called Clifford torus. The Clifford torus is conjectured to attain the minimum of the Willmore energy (1.4) among all genus 1 surfaces, see e.g. Willmore (1993). The Clifford torus is a standard torus with a ratio of large radius R and small radius r of $\frac{R}{r} = \sqrt{2}$, which leads to a Willmore energy of $E = 4\,\pi^2$. For the values in Table 13 we chose $r = 1$. Once again it appears to be clear that the approximation (4.3) of mean curvature does rather well, while the remaining definitions are not practical at all. Lastly, we also investigated how well the discrete Willmore energy based on the mean curvature κ^m computed from our scheme (2.7) approximates the true Willmore energy of a Clifford torus. To this end, we performed one step of our scheme (2.7) for the Clifford torus for different choices of κ^0 and report on $\frac{1}{2}\langle\kappa^1,\kappa^1\rangle_1^h$. Here we chose $\tau = 0.125\,h^2_{\vec{X}^0}$. The results can be seen in Table 14, where it appears that the computed κ^1 yields a better approximation than the initial κ^0. Moreover, in this case the discrete energy seems to converge as $h \to 0$ independently of the choice of κ^0.

K	$h_{\vec{X}^0}$	(4.3)	(4.2)	(4.4)
32	1.9734e-00	3.0480e+01	-6.7719e-00	4.2884e+01
128	1.1352e-00	5.4797e-00	2.0280e-00	1.0828e+01
512	5.8945e-01	6.5346e-01	2.1038e-01	3.2423e-01
2048	3.6083e-01	2.2686e-01	3.9266e-02	-1.3231e-00
8192	1.8165e-01	6.6494e-02	1.4837e-02	-9.0362e-01
32768	7.4729e-02	1.2720e-02	3.4571e-03	-2.4143e-01
131072	3.7371e-02	3.2274e-03	8.3623e-04	-6.8343e-02

Table 14: $\frac{1}{2}\langle\kappa^1,\kappa^1\rangle_1^h - 4\,\pi^2$ for (2.7) with different choices of κ^0.

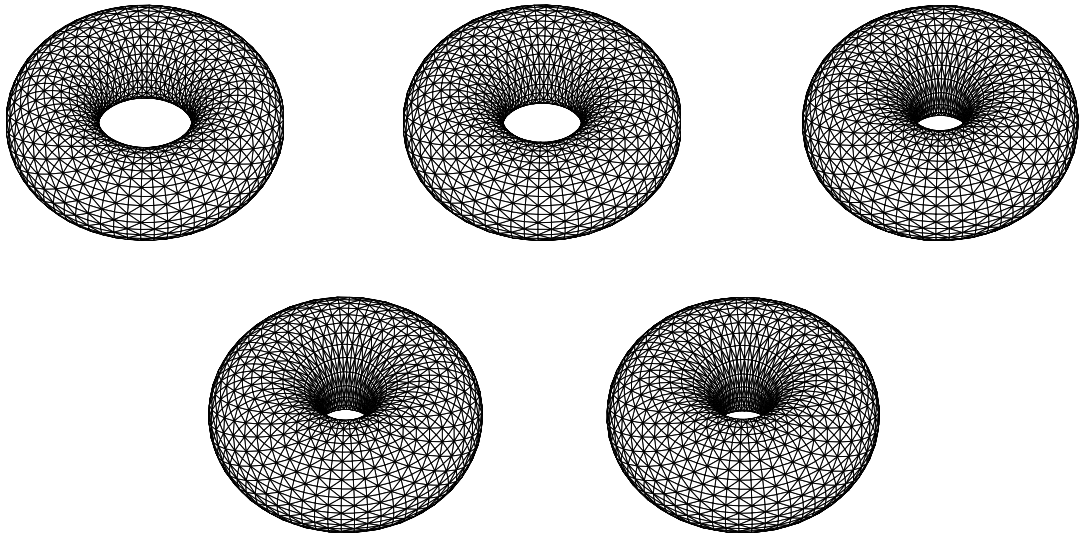

Figure 7: $\vec{X}(t)$ for $t = 0,\ 0.1,\ 0.5,\ 1,\ 2$.

Torus experiments

In our first evolution experiment we start with a torus of revolution with radii $R = 2$ and $r = 1$. We show the evolution in Figure 7. The chosen discretization parameters for the scheme (2.7), with (2.17a,b) and strategy (2.19)(i) with $\alpha = 0.5$, were $K = 2048$, $J = 4096$ and $\tau = 2\times10^{-4}$. We note that here we use $\alpha = 0.5$ in order to avoid undesirable vertex spiralling effects close to the hole of the torus, which can be observed for the choice $\alpha = 0$, i.e. the scheme (2.7), (2.4). See Figure 8 for a plot of the energy

$$E^m := \begin{cases} \frac{1}{2}\,\langle\kappa^{m+1},\kappa^{m+1}\rangle_m^h & m = 0 \to M-1, \\ \frac{1}{2}\,\langle\kappa^{M},\kappa^{M}\rangle_M^h & m = M, \end{cases} \tag{4.9}$$

which has reached a value $E^M = 39.4761827$ very close to $4\,\pi^2 \approx 39.4784176$ at time T. Note that the norm of the discrete normal velocity

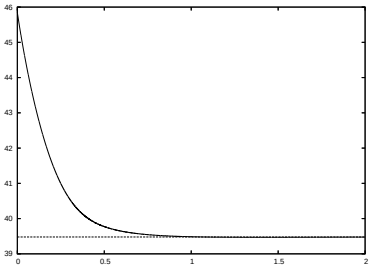

Figure 8: Plot of the energy E^m over time. It approaches the optimal value $4\,\pi^2$.

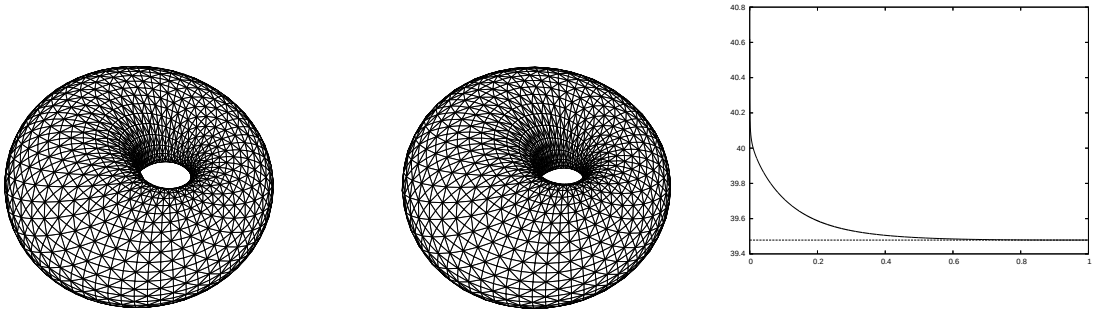

Figure 9: $\vec{X}(t)$ for $t = 0,\ 1$. A plot of E^m on the right.

$$\vartheta^{m+1} := \left| \frac{\vec{X}^{m+1} - \vec{X}^m}{\tau_m} \cdot \vec{\nu}^m \right|_{m,h} \tag{4.10}$$

has reached a value of $\vartheta^M = 5.2 \times 10^{-7}$.

In an experiment for a sickle torus, we used $R = 2$ with the small radius varying continuously in the interval $[1, 1.75]$. The evolution for this experiment can be seen in Figure 9. The discretization parameters were as in the experiment before. From the plot of the energy E^m we see that the numerical solution seems to have reached a conjectured optimal sickle torus configuration, i.e. a surface in the family of non axisymmetric conformal transformations of the Clifford torus, see e.g. Seifert (1997, p. 71). In fact, at time $T = 1$ it has reached $E^M = 39.4785147$, which is almost exactly equal to $4\,\pi^2$. We remark here that the Willmore energy is invariant under conformal mappings and that the optimal sickle torus can be obtained from the Clifford torus by a conformal transformation.

In a slightly more interesting evolution, we studied the Willmore flow of a much thinner non axisymmetric torus. Here the large radius was fixed to be $R = 5$, while the small radius varied continuously in the interval $[1, 3]$. The evolution for this experiment can be seen in Figure 10. The discretization parameters were as before, again for the scheme (2.7) with (2.17a,b) and (2.19)(i) with $\alpha = 0.5$. The discrete normal velocity at time $T = 30$ was $\vartheta^M = 6.3 \times 10^{-6}$ with the energy being $E^M = 39.5144845$, which is again very close to the optimal value $4\,\pi^2$.

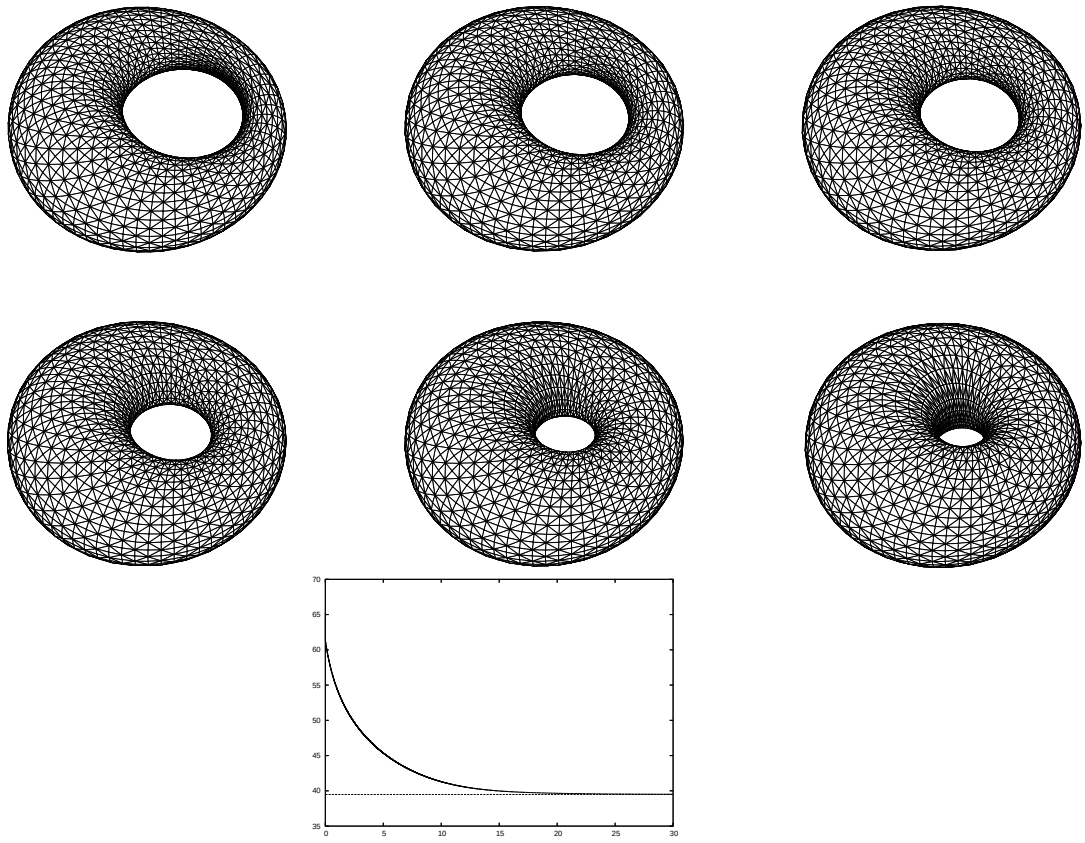

Figure 10: $\vec{X}(t)$ for $t = 0,\ 1,\ 2,\ 5,\ 10,\ 30$. A plot of E^m below.

Higher genus results

We start with an experiment for a genus 2 surface. The initial surface is given by a figure eight made up of unit cubes. The total dimensions of the initial surface are $7 \times 4 \times 1$. The results can be seen in Figure 11, where we used the scheme (2.7) and (2.4), with one step of the scheme (2.20) after each time step. Here, and whenever this redistribution strategy is employed, we recover the mean curvature discretization κ^m on the new triangulation Γ^m with the help of the analogue of (4.3) on Γ^m. The discretization parameters were $K = 2494$, $J = 4992$ and $\tau = 2 \times 10^{-4}$. The discrete Willmore energy at time $T = 4$ was $E^M = 45.038$. This is slightly larger than the value $43.8 = 2 \times 21.90$ reported in Hsu, Kusner, and Sullivan (1992, p. 202) for the same "button" surface, and the value $43.934 = \frac{1}{2}(113 - 8\,\pi)$ reported in Joshi and Sequin (2007, p. 615) for the so-called Lawson surface $\xi_{1,2}$ of genus 2, see Figure 12, below, for our approximation in this case. The different scalings occur, because the authors consider the equivalent free energies $\int_\Gamma (\frac{\varkappa}{2})^2 \,\mathrm{d}s = \frac{1}{2}\,E(\Gamma)$ and $\int_\Gamma (\varkappa_1^2 + \varkappa_2^2) \,\mathrm{d}s = \int_\Gamma \varkappa^2 \,\mathrm{d}s - 2\,\int_\Gamma \mathcal{K} \,\mathrm{d}s = 2\,E(\Gamma) - 8\,\pi\,(1-g)$, recall (1.11), respectively. We note that Hsu, Kusner, and Sullivan (1992) employ the Surface Evolver, see Brakke (1992), for their numerical experiments. In particular, they use a gradient descent approach for the energy (4.5), defined via (4.4), as a functional on the

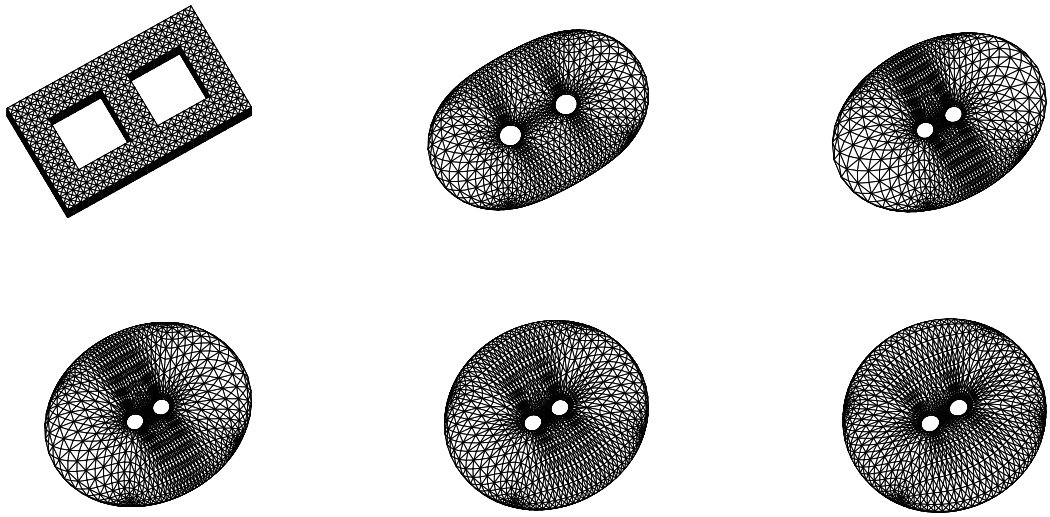

Figure 11: $\vec{X}(t)$ for $t = 0,\ 0.5,\ 1,\ 2,\ 3,\ 4$.

space $(\mathbb{R}^d)^K$ of position vectors for polyhedral surfaces. In Joshi and Sequin (2007), on the other hand, an involved quasi-Newton optimization for a discrete Willmore energy model on a smooth surface representation based on bi-cubic B-spline patches is employed. We stress that both of these approaches attempt to directly find minimizers of the Willmore energy (1.4), they do not compute solutions to the evolution equation (1.8).

In view of the results in Tables 12–14, it is quite possible that our apparent overestimation of the conjectured minimum value is due to the mesh not being sufficiently fine in our numerical experiment. Hence we uniformly refine the mesh obtained at time $T = 4$ and continue the evolution on that triangulation until the discrete energy has settled down. The new mesh has parameters $K = 9982$ and $J = 19968$ and settles down to an energy of 44.228 (after 1000 time steps of the same step size as before). After yet another refinement the mesh has $K = 39934$ vertices and $J = 79872$ elements and reaches an energy of 44.050 (after 60 time steps).

Finally for the genus 2 case, we also attempted an evolution towards Lawson's genus-two surface $\xi_{1,2}$, see e.g. Hsu, Kusner, and Sullivan (1992, Fig. 8), which the authors state is conformally equivalent to the previously computed "button" surface. We remark that Kusner (1989) conjectured that the Lawson surface $\xi_{1,g}$ minimizes the Willmore energy $E(\Gamma)$ among all surfaces of genus g. The results for the scheme (2.7) and one step of (2.20) after each time step can be seen in Figure 12. We used $K = 1854$, $J = 3712$ and $\tau = 2 \times 10^{-4}$. The computed energy at time $T = 1$ was $E^M = 44.449$. As in the experiment before, we continued the evolution on finer grids in order to obtain better estimates for the minimum Willmore energy of genus 2 surfaces. For a triangulation with $K = 7422$ and $J = 14848$, the discrete energy settles down to 43.968 (after 1000 time steps). After yet another refinement the mesh has $K = 29694$ vertices and $J = 59392$ elements and seems to settle on an energy of 43.855 (after 250 time steps). Interestingly,

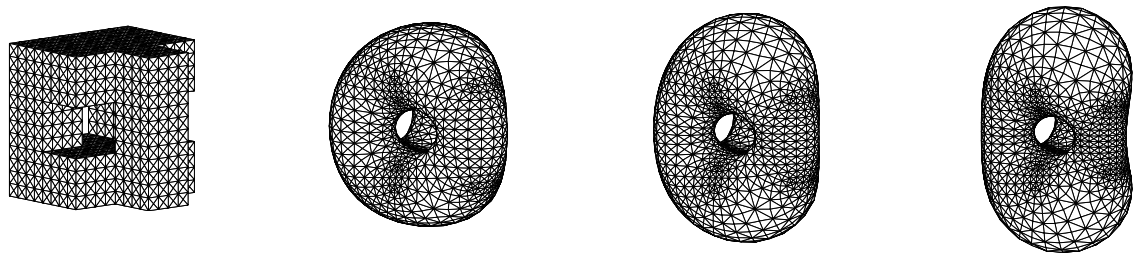

Figure 12: $\vec{X}(t)$ for $t = 0,\ 0.1,\ 0.5,\ 2$.

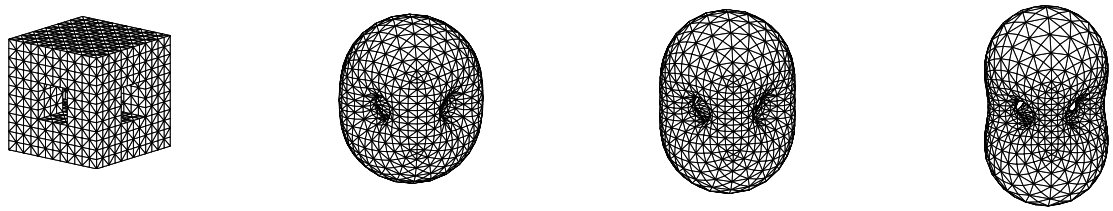

Figure 13: $\vec{X}(t)$ for $t = 0,\ 0.5,\ 1,\ 2$.

our numerical experiments seem to suggest that the surface approximated in Figure 12 has a smaller Willmore energy than the surface in Figure 11. However, unfortunately we are not in a position to be able to decide whether this difference is due to discretization errors or whether it is genuine. The numerical experiments in Hsu, Kusner, and Sullivan (1992) suggest that the two values should be the same, but these are based on the formulation (4.4), which does not appear reliable in our numerical tests.

We investigate also the evolution of a genus 3 surface under Willmore flow, and in particular study the flow towards Lawson's genus-three surface $\xi_{1,3}$. The dimensions of the initial surface are $3 \times 3 \times 3$, with the region enclosed by Γ^0 given as the union of 22 unit cubes. The numerical results can be seen in Figure 13. We use the scheme (2.7) with one step of (2.20) after each time step. The discretization parameters were $K = 1084$, $J = 2176$ and $\tau = 10^{-3}$. The discrete Willmore energy at time $T = 2$ is $E^M = 46.498$. This compares with the values $45.64 = 2 \times 22.82$ reported in Hsu, Kusner, and Sullivan (1992) and $45.867 = \frac{1}{2}\,(142 - 16\,\pi)$ reported in Joshi and Sequin (2007) for approximations of the surface $\xi_{1,3}$. Again we used a refined mesh of our solution at time $T = 2$ in order to better estimate its Willmore energy. The refined mesh has parameters $K = 4348$ and $J = 8704$ and the energy settles on a value of 45.858 (after 1000 time steps). The next finer mesh has $K = 17404$ vertices and $J = 34816$ elements. The energy on this mesh reaches a value of 45.696 (after 800 time steps).

Next we investigate the evolution of a genus 5 surface under Willmore flow. Similarly to the surface in Figure 13, the initial surface is given as the boundary of the union of 20 unit cubes, so that the total dimensions are $3 \times 3 \times 3$. We used the same discretization parameters as before, except that the mesh here consists of $K = 1144$ vertices and $J =$

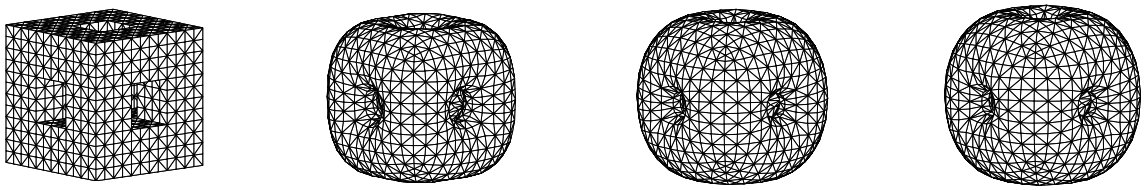

Figure 14: $\vec{X}(t)$ for $t = 0,\ 0.05,\ 0.5,\ 1$.

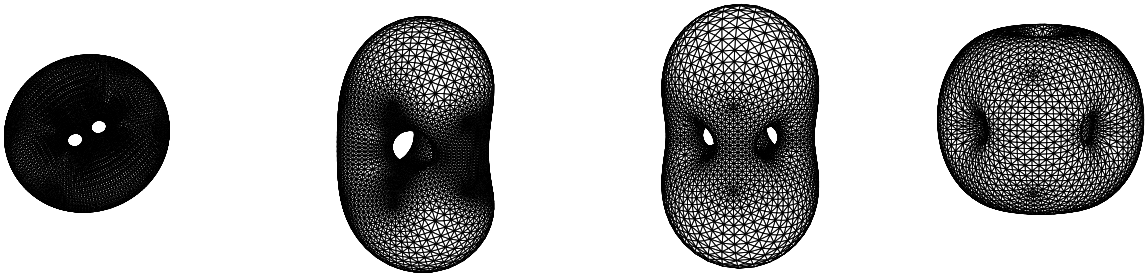

Figure 15: Fine meshes for genus 2, 3 and 5 surfaces. These meshes have $K = 9982$, $K = 7422$, $K = 4348$ and $K = 4600$ vertices, respectively.

2304 elements. The results can be seen in Figure 14. The discrete Willmore energy at time $T = 1$ is $E^M = 50.711$. This compares with the value $49.235 = \frac{1}{2}(199 - 32\,\pi)$ reported in Joshi and Sequin (2007). However, we observe that significantly smaller values of $47.32 = 2 \times 23.66$ and $47.235 = \frac{1}{2}(195 - 32\,\pi)$ have been reported in Hsu, Kusner, and Sullivan (1992) and Joshi and Sequin (2007) for a different type of genus 5 surface. In order to better estimate the Willmore energy of the surface produced by our approximation, we refined the mesh obtained at time $T = 1$ to start a new evolution. The refined mesh has parameters $K = 4600$ and $J = 9216$. The energy reaches a value of 49.382 (after 1000 time steps). The next finer mesh consists of $K = 18424$ vertices and $J = 36864$ elements. On this triangulation, the energy settles on a value of 49.103 (after 1000 time steps).

The refined meshes for the last genus 2, 3 and 5 experiments can be seen in Figure 15, where we observe that the smooth surface they approximate appears to be the same as that for the coarser grids on which the evolutions were computed. Hence we are satisfied that the overestimation in the discrete Willmore energy for these coarser meshes is purely due to the discretization error in computing the Willmore energy; similarly to the behaviour observed in Tables 12–14.

4.2.5 Helfrich flow and other models

We report on an experiment for the Helfrich flow of an initial tube of total dimensions $4 \times 1 \times 1$. The discretization parameters were $K = 1154$, $J = 2304$ and $\tau = 10^{-3}$. See Figure 16 for the results, where at time $T = 1$ the evolution has almost reached a

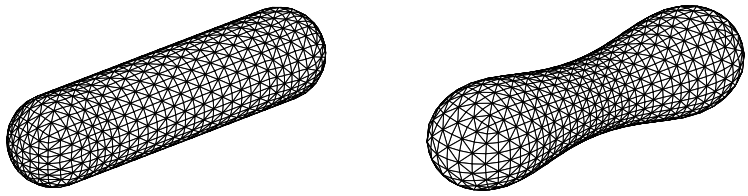

Figure 16: $\vec{X}(t)$ for $t = 0,\ 1$.

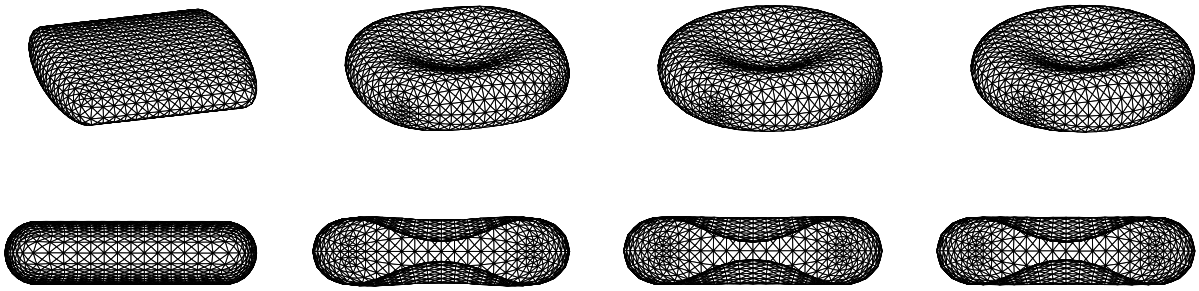

Figure 17: $\vec{X}(t)$ for $t = 0,\ 0.1,\ 0.25,\ T = 0.5$. Below the corresponding cross-sections.

numerical steady state, e.g. $\vartheta^M = 3 \times 10^{-8}$, recall (4.10). Note that at time $T = 1$ the relative area loss was -0.72% while the relative volume loss was -0.55%. Similarly, in Figures 17 and 18 we show the evolution for initially elliptical tubes of total dimensions $4 \times 4 \times 1$ and $5 \times 5 \times 1$, respectively. We can see that while the former evolution leeds to a shape resembling a human blood cell, the latter evolution produces a surface with self intersection. Of course, in real life this would yield a change in topology to a torus. The discretization parameters for the scheme (2.8) with (2.17a,b), (2.19)(i) and $\alpha = 0.5$ for both experiments were $K = 1122$, $J = 2240$, $\tau = 2 \times 10^{-4}$ and $T = 0.5$. At time $t = T$ we found $\vartheta^M = 3.5 \times 10^{-7}$ and $\vartheta^M = 2 \times 10^{-6}$, respectively, with the relative losses in area and volume -0.26% and -0.08% for the former and 0.1% and -0.05% for the latter experiment.

Next we investigated the evolution towards an oblate symmetric steady state solution, as reported in e.g. Ziherl and Svetina (2005), see also Heinrich, Svetina, and Zeks (1993) and Wintz, Döbereiner, and Seifert (1996). To this end we started with an elliptical tube, with total dimensions $4 \times 2 \times \frac{3}{4}$ and kept all the discretization parameters as before, except $K = 1154$ and $J = 2304$. The results can be seen in Figure 19. For this experiment we observed $\vartheta^M = 4.3 \times 10^{-7}$, with the relative losses in area and volume -0.32% and -0.13%.

Next we compute evolutions for the model (1.14), employing our scheme (2.8) with $\varrho > 0$. In the first computation, we repeated the experiment in Figure 16, but now with $\varrho = 10$ and either $M_0 = \langle \kappa^0, 1 \rangle_0 \approx -31.26$, $M_0 = -28$ or $M_0 = -33$. The results can be

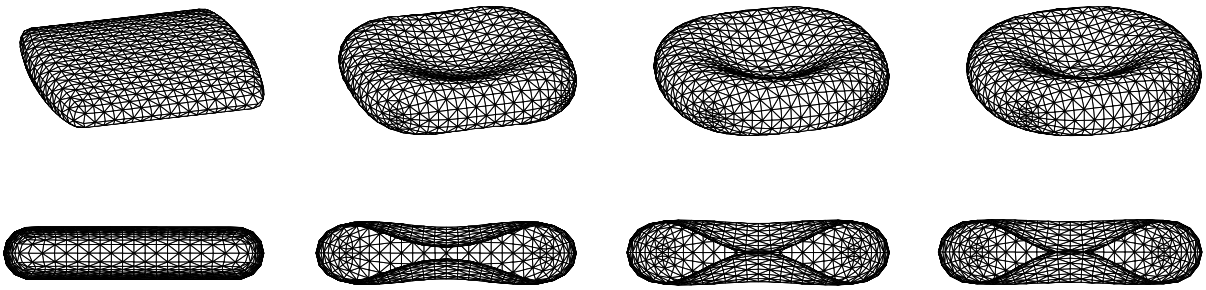

Figure 18: $\vec{X}(t)$ for $t = 0,\ 0.1,\ 0.25,\ T = 0.5$. Below the corresponding cross-sections.

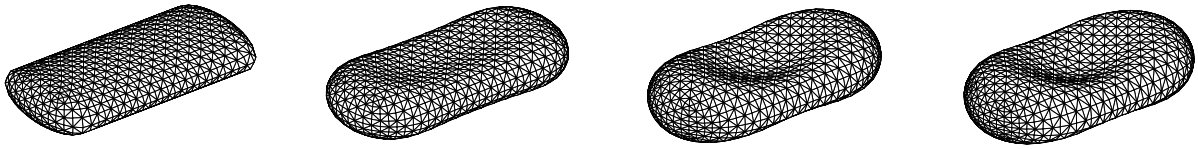

Figure 19: $\vec{X}(t)$ for $t = 0,\ 0.01,\ 0.1,\ T = 0.5$.

seen in Figure 20, where we used the same discretization parameters as in the experiment for Figure 16, apart from the run for $M_0 = -28$, where we used (2.19)(i) with $\alpha = 0.1$ in order to suppress unwanted tangential movement of vertices. We note that the first shape is very oblate, with the second shape being slightly oblate, while the last surface features a pronounced neck.

4.2.6 Spontaneous curvature effects

In this subsection, we consider flows for the free energy (1.12) with $\overline{\varkappa} < 0$. For our sign convention and convex surfaces this means that a sphere of radius $\frac{2}{|\overline{\varkappa}|}$ will be the global energy minimizer with $E(\Gamma) = 0$. As a first experiment, and for a value $\overline{\varkappa} = -2$, we choose as initial surface a tube of total dimensions $6 \times 2 \times 2$ and set the discretization parameters for the scheme (2.7) to $K = 898$, $J = 1792$ and $\tau = 10^{-3}$. The evolution is

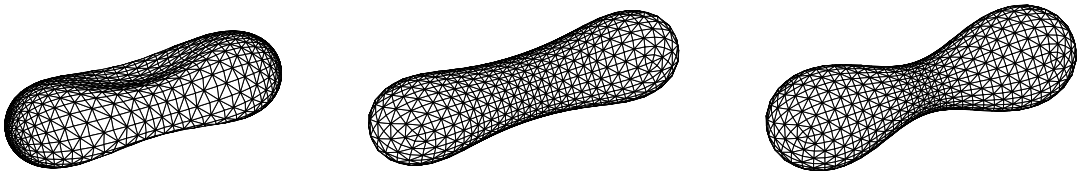

Figure 20: $\vec{X}(1)$ for $M_0 = -28$, $M_0 \approx -31.26$ and $M_0 = -33$.

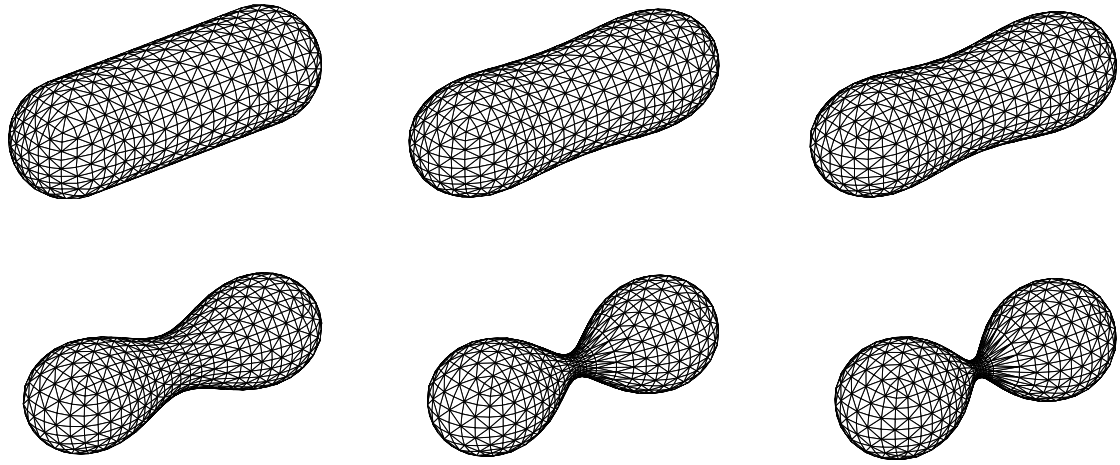

Figure 21: Flow with $\overline{\varkappa} = -2$. $\vec{X}(t)$ for $t = 0,\ 0.05,\ 0.1,\ 0.25,\ 0.5,\ 1$.

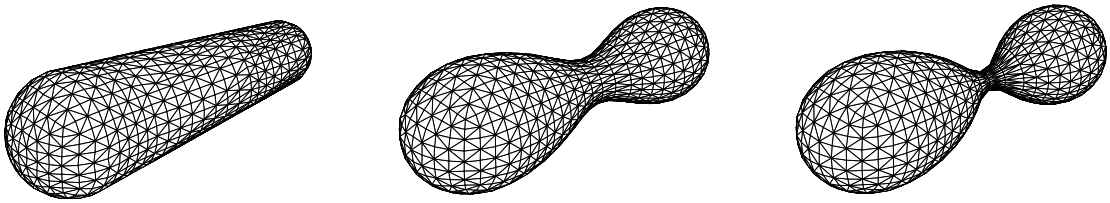

Figure 22: Flow with $\overline{\varkappa} = -3$ and volume preservation. $\vec{X}(t)$ for $t = 0,\ 0.1,\ 0.115$.

shown in Figure 21. We can see that the tube evolves towards a dumbbell consisting of two "spheres" with radius close to unity. The limiting shape of this evolution is singular and consists of two unit spheres touching each other at a single point. This singular shape is beyond our direct approximation. We note that the same experiment with $\overline{\varkappa} = 0$ would yield a smooth evolution to a single sphere.

In a similar experiment, we started with a cigar like shape that has a smaller radius on the right hand side. The Willmore flow with spontaneous curvature $\overline{\varkappa} = -3$ and enforced volume preservation can be seen in Figure 22, where we kept all the discretization parameters the same, except $T = 0.115$. Shortly after this, the surface tries to pinch off. The same experiment without volume preservation is shown in Figure 23, where we can see that three touching spheres evolve.

Next we repeated the experiment in Figure 18, again for a value of $\overline{\varkappa} = -2$. The new evolution, this time for the scheme (2.8) with (2.4), can be seen in Figure 24, where we can see that the four corners of the shape evolve into four "spheres" of radius close to unity. At time $T = 0.22$, the discrete normal velocity was 4×10^{-5}, and the relative losses in area and volume were 0.28% and -0.03%, respectively. We note that the star fish like shape produced in Figure 24 looks very similar to the shape reported in Wintz,

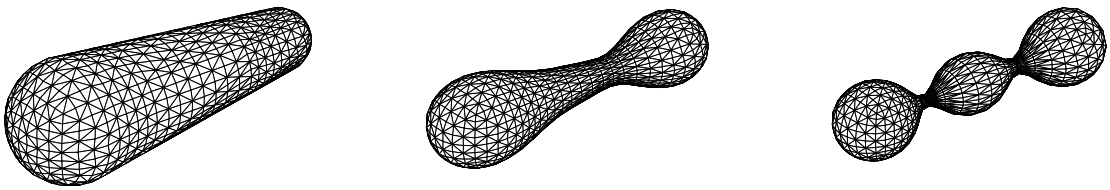

Figure 23: Flow with $\overline{\varkappa} = -3$ without volume preservation. $\vec{X}(t)$ for $t = 0,\ 0.1,\ 0.21$.

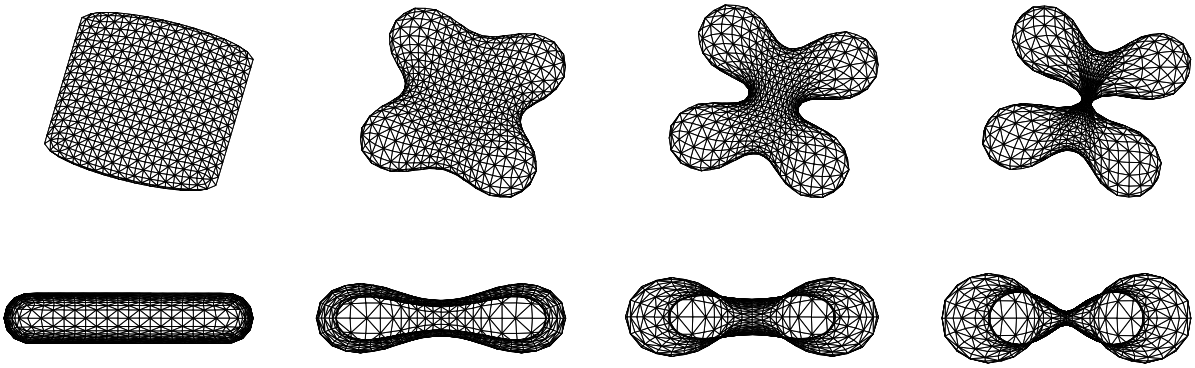

Figure 24: Flow with $\overline{\varkappa} = -2$. $\vec{X}(t)$ for $t = 0,\ 0.05,\ 0.1,\ 0.15,\ 0.22$. Below the corresponding cross-sections.

Döbereiner, and Seifert (1996, Fig. 2).

In an attempt to compute a 7-fingered star shape, as e.g. reported in Wintz, Döbereiner, and Seifert (1996, Fig. 1), we start the next computation with an elliptic surface based on a $5 \times 5 \times \frac{3}{4}$ ellipsoid, where the "radius" varies continuously between 1 ± 0.05. Here we employed an initial triangulation that uses finer elements in regions of high curvature. The chosen discretization parameters for the scheme (2.8) were $K = 2314$, $J = 4624$ and $\tau = 10^{-3}$. The spontaneous curvature was set to $\overline{\varkappa} = -2$. For the results see Figure 25. Once again we observe the good agreement with the surfaces reported in Wintz, Döbereiner, and Seifert (1996).

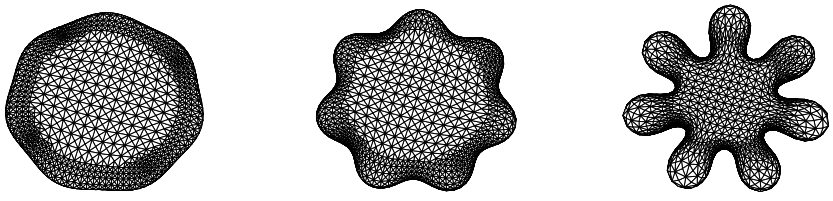

Figure 25: Flow with $\overline{\varkappa} = -2$. $\vec{X}(t)$ for $t = 0,\ 0.2,\ 0.42$.

References

Andrews, B. (2000). Motion of hypersurfaces by Gauss curvature. *Pacific J. Math. 195*(1), 1–34.

Bänsch, E., P. Morin, and R. H. Nochetto (2005). A finite element method for surface diffusion: the parametric case. *J. Comput. Phys. 203*(1), 321–343.

Barrett, J. W., H. Garcke, and R. Nürnberg (2006). On the parametric finite element approximation of evolving hypersurfaces in $\mathbb{R}^3$. Preprint No. 18/2006, University Regensburg, Germany.

Barrett, J. W., H. Garcke, and R. Nürnberg (2007). A parametric finite element method for fourth order geometric evolution equations. *J. Comput. Phys. 222*(1), 441–467.

Bauer, M. and E. Kuwert (2003). Existence of minimizing Willmore surfaces of prescribed genus. *Int. Math. Res. Not. 2003*(10), 553–576.

Brakke, K. A. (1992). The surface evolver. *Experiment. Math. 1*(2), 141–165.

Chopp, D., L. C. Evans, and H. Ishii (1999). Waiting time effects for Gauss curvature flows. *Indiana Univ. Math. J. 48*(1), 311–334.

Clarenz, U., U. Diewald, G. Dziuk, M. Rumpf, and R. Rusu (2004). A finite element method for surface restoration with smooth boundary conditions. *Comput. Aided Geom. Design 21*(5), 427–445.

Daskalopoulos, P. and R. Hamilton (1999). The free boundary in the Gauss curvature flow with flat sides. *J. Reine Angew. Math. 510*, 187–227.

Daskalopoulos, P. and K. Lee (2001). Free-boundary regularity on the focusing problem for the Gauss curvature flow with flat sides. *Math. Z. 237*(4), 847–874.

Deckelnick, K. and G. Dziuk (2006). Error analysis of a finite element method for the Willmore flow of graphs. *Interfaces Free Bound. 8*(1), 21–46.

Deckelnick, K., G. Dziuk, and C. M. Elliott (2005). Computation of geometric partial differential equations and mean curvature flow. *Acta Numer. 14*, 139–232.

Di Carlo, A., M. E. Gurtin, and P. Podio-Guidugli (1992). A regularized equation for anisotropic motion-by-curvature. *SIAM J. Appl. Math. 52*(4), 1111–1119.

Dziuk, G. (1991). An algorithm for evolutionary surfaces. *Numer. Math. 58*(6), 603–611.

Dziuk, G., E. Kuwert, and R. Schätzle (2002). Evolution of elastic curves in $\mathbb{R}^n$: existence and computation. *SIAM J. Math. Anal. 33*, 1228–1245.

Ecker, K. (2004). *Regularity Theory for Mean Curvature Flow*. Boston: Birkhäuser.

Firey, W. J. (1974). Shapes of worn stones. *Mathematika 21*, 1–11.

Garcke, H. and S. Wieland (2006). Surfactant spreading on thin viscous films: nonnegative solutions of a coupled degenerate system. *SIAM J. Math. Anal. 37*, 2025–2048.

Gurtin, M. E. (1993). *Thermomechanics of Evolving Phase Boundaries in the Plane*. New York: Oxford University Press.

Gurtin, M. E. and M. E. Jabbour (2002). Interface evolution in three dimensions with curvature-dependent energy and surface diffusion: interface-controlled evolution, phase transitions, epitaxial growth of elastic films. *Arch. Ration. Mech. Anal. 163*(3), 171–208.

Heine, C.-J. (2007). Isoparametric finite element approximation of curvature on hypersurfaces. Preprint, University Freiburg.

Heinrich, V., S. Svetina, and B. Zeks (1993, Oct). Nonaxisymmetric vesicle shapes in a generalized bilayer-couple model and the transition between oblate and prolate axisymmetric shapes. *Phys. Rev. E 48*(4), 3112–3123.

Helfrich, W. (1973). Elastic properties of lipid bilayers: Theory and possible experiments. *Z. Naturforsch. 28c*, 693–703.

Hsu, L., R. Kusner, and J. Sullivan (1992). Minimizing the squared mean curvature integral for surfaces in space forms. *Experiment. Math. 1*(3), 191–207.

Joshi, P. and C. Sequin (2007). Energy minimizers for curvature-based surface functionals. *Comput. Aided Design Appl. 4*(5), 607–617.

Kusner, R. (1989). Comparison surfaces for the Willmore problem. *Pacific J. Math. 138*(2), 317–345.

Kuwert, E. and R. Schätzle (2001). The Willmore flow with small initial energy. *J. Differential Geom. 57*(3), 409–441.

Kuwert, E. and R. Schätzle (2002). Gradient flow for the Willmore functional. *Comm. Anal. Geom. 10*(2), 307–339.

Kuwert, E. and R. Schätzle (2004). Removability of point singularities of Willmore surfaces. *Ann. of Math. (2) 160*(1), 315–357.

Mayer, U. F. and G. Simonett (2002). A numerical scheme for axisymmetric solutions of curvature-driven free boundary problems, with applications to the Willmore flow. *Interfaces Free Bound. 4*(1), 89–109.

Meek, D. S. and D. J. Walton (2000). On surface normal and Gaussian curvature approximations given data sampled from a smooth surface. *Comput. Aided Geom. Design 17*(6), 521–543.

Pinkall, U. and I. Sterling (1987). Willmore surfaces. *Math. Intelligencer 9*(2), 38–43.

Rusu, R. E. (2005). An algorithm for the elastic flow of surfaces. *Interfaces Free Bound. 7*(3), 229–239.

Schmidt, A. and K. G. Siebert (2005). *Design of Adaptive Finite Element Software: The Finite Element Toolbox ALBERTA*, Volume 42 of *Lecture Notes in Computational Science and Engineering*. Berlin: Springer-Verlag.

Schnürer, O. C. (2006). Surfaces expanding by the inverse Gauß curvature flow. *J. Reine Angew. Math. 600*, 117–134.

Seifert, U. (1997). Configurations of fluid membranes and vesicles. *Adv. Phys. 46*, 13–137.

Sullivan, J. (2002). Curvature measures for discrete surfaces. Oberwolfach, Preprint, `http://torus.math.uiuc.edu/jms/Papers/`.

Svetina, S. and B. Zeks (1983). Bilayer couple hypothesis of red cell shape transformations and osmotic hemolysis. *Biomed. Biochim. Acta 42*, 86–90.

Tso, K. (1985). Deforming a hypersurface by its Gauss-Kronecker curvature. *Comm. Pure Appl. Math. 38*(6), 867–882.

Ushijima, T. K. and H. Yagisita (2005). Convergence of a three-dimensional crystalline motion to Gauss curvature flow. *Japan J. Indust. Appl. Math. 22*(3), 443–459.

Willmore, T. J. (1965). Note on embedded surfaces. *An. Şti. Univ. "Al. I. Cuza" Iaşi Secţ. I a Mat. (N.S.) 11B*, 493–496.

Willmore, T. J. (1993). *Riemannian geometry*. Oxford Science Publications. New York: The Clarendon Press Oxford University Press.

Wintz, W., H.-G. Döbereiner, and U. Seifert (1996). Starfish vesicles. *Europhys. Lett. 33*, 403–408.

Zhao, H. and G. Xu (2006). Triangular surface mesh fairing via Gaussian curvature flow. *J. Comput. Appl. Math. 195*(1-2), 300–311.

Ziherl, P. and S. Svetina (2005). Nonaxisymmetric phospholipid vesicles: Rackets, boomerangs, and starfish. *Europhys. Lett. 70*(5), 690–696.